

Spin and Spin Current — From Fundamentals to Recent Progresses

Sadamichi Maekawa,^{1, 2, 3, a)} Takashi Kikkawa,⁴ Hiroyuki Chudo,² Jun'ichi Ieda,² and Eiji Saitoh^{2, 4, 5, 6, b)}

¹⁾Center for Emergent Matter Science (CEMS), RIKEN, Wako 351-0198, Japan

²⁾Advanced Science Research Center, Japan Atomic Energy Agency, Tokai 319-1195, Japan

³⁾Kavli Institute for Theoretical Sciences, University of Chinese Academy of Sciences, Beijing, 100190, China

⁴⁾Department of Applied Physics, The University of Tokyo, Tokyo 113-8656, Japan

⁵⁾Institute for AI and Beyond, The University of Tokyo, Tokyo 113-8656, Japan

⁶⁾WPI Advanced Institute for Materials Research, Tohoku University, 980-8577, Japan

(Dated: 7 November 2022)

Along with the progress of the spin science and spintronics research, the flow of electron spins, *i.e.*, spin current, has come to attract attention. New phenomena and electronic states were explained one after another using the concept of spin current. Moreover, as many of the conventionally known spintronics phenomena became well organized based on spin current it has rapidly been recognized as an essential concept in a wide range of condensed matter physics. In this article, we focus on recent developments in the physics of spin, spin current, and their related phenomena, where the conversion between spin angular momentum and different forms of angular momentum plays an essential role. Starting with an introduction to spin current, we first discuss the recent progress in the spintronic phenomena driven by spin-exchange coupling: spin pumping, topological Hall torque, and emergent inductor. We then extend our discussion to the interaction/interconversion of spins with heat, lattice vibrations, and charge current and address recent progress and perspectives on the spin Seebeck and Peltier effects. Next, we review the interaction between mechanical motion and electron/nuclear spins and argue the difference between the Barnett field and the rotational Doppler effect. We show that the Barnett effect reveals the angular momentum compensation temperature, at which the net angular momentum is quenched in ferrimagnets.

I. INTRODUCTION

In electronics, various functions have been realized by controlling the electric charge (electricity) and electric current. Electronics has become an indispensable technology in every aspect of daily life such as home appliances and information and communication devices in modern society. An electron is an elementary particle that carries electric charge and spin. However, electronics has used only the electric charge. The research field that has used electron spins has been magnetics. Thus, the two properties of an electron, charge and spin, were studied and utilized separately in electronics and magnetics, respectively. This situation was changed by the great progress of nanotechnology in 1990's, and the construction of electronic devices that effectively connect and use the electric charge and spin of electrons has begun.

Spin is an intrinsic nature of an electron which is associated with angular momentum, $\hbar/2$, and magnetic moment, $e\hbar/2m_e$, where e , \hbar , m_e , and c represent the electron charge, Planck constant divided by 2π , electron mass, and light velocity, respectively. The spins interact each other and align when they are in a ferromagnet. Another intrinsic one of an electron is charge, e , which is utilized in electronics. Oxford dictionary defines electronics as “the branch of physics and technology concerned with the design of circuits using transistors and microchips, and with the behavior and movement of electrons in a semiconductor, conductor, vacuum, or gas.” Here, “movement of electrons” means “the movement of electron charges.”

The electron spins can also flow in a material, independently of their charges. This is called *spin current*^{1,2}. Since the beginning of this century, special attention has been paid to spin current and *spin accumulation* in semiconductors, metals and even insulators, and to how to utilize them together with electric charge current. This field of research and applications is named *spintronics* in contrast with electronics.

The flows of spin and charge of electrons can couple each other due to the spin-orbit coupling (SOC) as well as the electromagnetic interaction. As a result, spin current and electric current may convert each other. The interconversion between the currents is called *spin Hall effect* (SHE) and *inverse spin Hall effect* (ISHE)^{3–8}, and is one of the keys in spintronics. In parallel to these findings, the discovery of *spin-transfer torque* (STT)^{9–12} brought about significant advances in applications of spin current for magnetic memory technology. In addition, it was shown recently that spin and charge interact due to the geometrical effect which is called *spin Berry phase*^{13–15}. The spin Berry phase also gives rise to a variety of the interconversion of spin and charge. This is also a key in spintronics.

It is known that nuclei such as protons and neutrons have spin angular momenta which are of the same order of magnitude of electron spins, although their magnetic moments μ_N are smaller by three orders of magnitude than that of an electron μ_e ($\mu_N/\mu_e = m_e/m_N \sim 10^{-3}$ with m_N being the mass of a proton). Therefore, considering the angular momentum conservation in a material, nuclear spins may contribute to a variety of physical properties in a material. The conservation may also include the angular momenta of mechanical motion and vortices of the flow of the constituents of a material. This suggests that spins of electrons couple to the mechanical motions of a material.

The purpose of this article is to discuss various aspects of

^{a)}Electronic mail: sadamichi.maekawa@riken.jp

^{b)}Electronic mail: eizi@ap.t.u-tokyo.ac.jp

materials based on the angular momentum conservation law including not only electron spins but nuclear spins and mechanical motion. In the second section, the concepts of spin current, spin accumulation and other quantities activating in spintronics are explained. In the third section, the interaction and interconversion of spin current and charge current are discussed. The generalization of the Faraday's law of electromagnetic induction to spintronics is presented¹⁶. In the fourth section, the interaction of spins with heat, lattice vibrations and electric current is introduced. Recent progress in and perspectives on the spin Seebeck and Peltier effects, which are two representative spin-heat coupling phenomena, are overviewed here. The behavior of nuclear spins is examined in connection with that of electron spins as well. In the fifth section, the interaction between mechanical motion and electron/nuclear spins is examined. The interaction is called the Einstein-de Hass effect¹⁷ whose inverse is the Barnett effect¹⁸. These interactions were discovered in 1915, but have not received much attention until recently. The topics in this section present recent experiments and perspectives of these effects. The last section summarizes the present article.

II. CONCEPT OF SPIN CURRENT

A. Conduction electron spin current

When an electric field is applied to a conductor, there is a slight difference in the amount of electrons having a velocity component parallel to the electric field and electrons having an antiparallel velocity component. Due to this slight imbalance in the velocity distribution of electrons, a group of electrons flows in a certain direction, which is an electric (charge) current [Fig. 1(a)]. Then, what would happen, when the electrons traveling in the opposite direction tend to have spins in opposite directions [Fig. 1(b)]? When the number of electrons traveling in both directions is the same, the charge flows cancel out each other and the net current is zero. By contrast, the spin flow remains uncanceled. This imbalance increases the upward spin on the right edge of the sample and reduces the upward spin at the left end, and thus there is an upward spin flow from left to right. (This can be rephrased as a downward spin flow from right to left.) In this way, by introducing such imbalance, it is possible to create only the spin flow with the zero current. This is a spin current carried by conduction electrons, which is called conduction-electron spin current [Fig. 1(b)]. The spin z component of the spin current is expressed as

$$\mathbf{J}_s = \mathbf{j}_\uparrow - \mathbf{j}_\downarrow. \quad (1)$$

The current $\mathbf{j}_{\uparrow(\downarrow)}$ represents a particle flow carrying the upward (downward) spin. By contrast, a charge current is described as

$$\mathbf{J}_c = \mathbf{j}_\uparrow + \mathbf{j}_\downarrow. \quad (2)$$

Here we introduce the spin dependent chemical potentials, μ_\uparrow

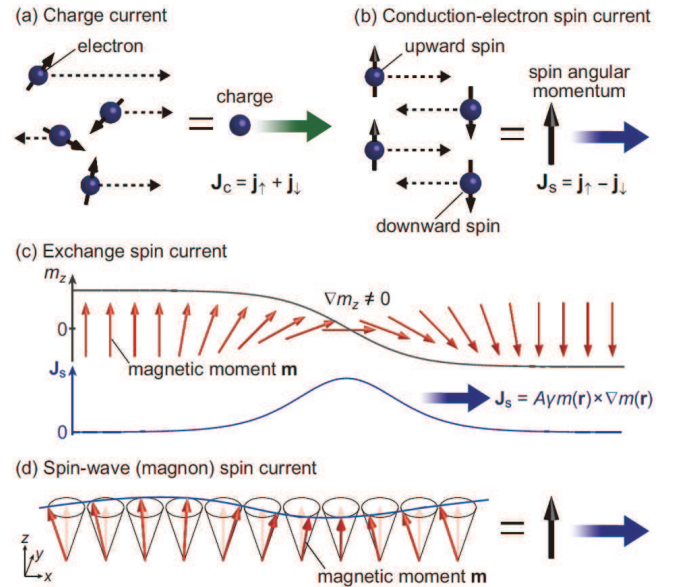


FIG. 1. Schematic illustrations of the (a) charge current, (b) conduction-electron spin current, (c) exchange spin current, and (d) spin-wave (magnon) spin current.

and μ_\downarrow , which satisfy

$$\mathbf{j}_{\uparrow(\downarrow)} = D \nabla \mu_{\uparrow(\downarrow)}, \quad (3)$$

where D is the electron diffusion constant. By using $\mu_{\uparrow(\downarrow)}$, the spin current \mathbf{J}_s can be written as

$$\mathbf{J}_s = D \nabla (\mu_\uparrow - \mu_\downarrow). \quad (4)$$

This shows that $(\mu_\uparrow - \mu_\downarrow)$ acts as a driving force for conduction electron spin current. In fact, since the spin current is not a conservative flow, it is difficult to transport the spin current over a long distance. This is a decisive difference from a charge current. Since a charge current is a conservative current, if a current is passed through one end of a metal wire, the same current can be taken out from the other end, unless the wire is charged because of the charge conservation law. By contrast, there is no such strong conservation law for spin, and there is a certain probability that the direction of spin will naturally change to disorder. As a result, the conduction electron spin current disappears after flowing over a certain distance, which is called the spin diffusion length. On a scale sufficiently shorter than the spin diffusion length, the spin current can be regarded as an approximate conservative current and can be expressed in the same way as the charge current.

Note that, in a strict sense, the physics of spin current cannot be constructed in exactly the same way as electric current. In fact, as described below, the definition of spin current is not uniquely determined because the conservation law does not hold exactly for spin, and there remains a big problem in the accurate definition of spin current. Nevertheless, by introducing the concept of spin current, new physical phenomena have been discovered one after another, and, conversely, the discovery of new physical phenomena greatly advances the

understanding of spin current. The concept of spin current becomes widespread as a powerful guiding principle for development of modern (condensed matter) physics.

Let us define the spin current under the assumption that the spin is a good quantum number and the spin angular momentum is fully conserved. In general, the magnetic moment of electrons carries the angular momentum, where the ratio is given by the gyromagnetic ratio γ (< 0). Then, the angular momentum conservation is written as

$$\frac{\partial}{\partial t} \mathbf{M}(\mathbf{r}, t) = -\gamma \operatorname{div} \mathbf{J}_s(\mathbf{r}, t), \quad (5)$$

where \mathbf{M} , \mathbf{r} , and t denote the local magnetization (magnetic-moment density), the position of the electron, and time, respectively. This equation shows that when \mathbf{J}_s changes spatially in a magnet, the magnetization receives torque (spin transfer torque) and it starts rotating. Equation (5) can be used as an acceptable approximation on a microscale, where the conservation of spin angular momentum is considered to be approximately valid. However, we need to keep in mind that, in general, the law of conservation of spin angular momentum does not hold to some extent.

B. Spin relaxation

Next, let us consider that the spin is not conserved. The simplest phenomenological expression of spin relaxation is

$$\mathbf{T} = -\frac{\mathbf{M}(\mathbf{r}) - \mathbf{M}_0}{\tau}, \quad (6)$$

where τ is the spin relaxation time. If this relaxation term is incorporated, Eq. (5) becomes

$$\frac{\partial}{\partial t} \mathbf{M}(\mathbf{r}) = -\gamma \operatorname{div} \mathbf{J}_s + \mathbf{T}. \quad (7)$$

The mechanism of spin relaxation in actual materials is very complicated. To date, several models of spin relaxation mechanisms have been proposed. As a typical model, there is a mechanism proposed by D'yakonov and Perel¹⁹. In this model, electron spins undergo precessional rotational motion due to the spin-orbit interaction, and the direction of precession changes as the direction of motion changes due to the scattering of electrons during orbital motion. In this model, a longer electron scattering time allows the spins to rotate by a larger angle, resulting in a stronger spin relaxation. Using an approximation with a high electron scattering frequency, the spin relaxation time is given by

$$\frac{1}{\tau} \sim \omega^2 \tau_p, \quad (8)$$

where ω is the angular frequency of spin precession, and τ_p is the momentum relaxation time of the electron. Besides, when conduction electrons are scattered, their spin can flip with the help of the spin-orbit interaction. This is called the Elliott—Yafet mechanism^{20,21}. In this mechanism, spin relaxation strength is proportional to electron scattering probability, $1/\tau \propto 1/\tau_p$.

The existence of spin relaxation obscures the definition of spin current as discussed above. The conserved current is uniquely determined by the continuity equation. However, the spin current has a relaxation term, and the continuity equation [Eq. (5)] does not hold as it is, which makes it impossible to accurately define the spin current. Any term extracted from \mathbf{T} can be added to spin current \mathbf{J}_s . In such cases, the definition of spin current has been used properly depending on the object to be considered, on a case-by-case basis.

C. Exchange spin current

An equation of motion for magnetization is given by

$$\frac{d}{dt} \mathbf{m} = -\gamma \mathbf{m} \times \mathbf{H}_{\text{eff}}. \quad (9)$$

Here, \mathbf{m} denotes the magnetic moment per a volume and \mathbf{H}_{eff} represents the effective field acting on \mathbf{m} ,

$$\mathbf{H}_{\text{eff}} = \frac{\delta E(\mathbf{m})}{\delta \mathbf{m}}, \quad (10)$$

where $E(\mathbf{m})$ is the total magnetic energy. Let us consider the effective magnetic field due to the ferromagnetic (Heisenberg) exchange interaction,

$$\mathcal{H} = -2J \sum_{\langle i,j \rangle} \mathbf{S}_i \cdot \mathbf{S}_j, \quad (11)$$

where \mathbf{S}_i is the spin of the i -th lattice site, J is called the exchange interaction constant, and the sum is taken over the nearest neighbor pairs. The effective field at the site i thereby reads as

$$\mathbf{H}_{\text{eff},i} = -2\frac{J}{\gamma} \sum_{\langle i,j \rangle} \mathbf{S}_j. \quad (12)$$

Substituting Eq. (12) into the equation of motion [Eq. (9)] yields

$$\frac{d}{dt} \mathbf{m} = 2J \mathbf{m} \times \sum_{\langle i,j \rangle} \mathbf{S}_j. \quad (13)$$

By using continuum approximation,

$$\mathbf{S}(\mathbf{r} + \mathbf{a}) = \mathbf{S}(\mathbf{r}) + \frac{\partial \mathbf{S}(\mathbf{r})}{\partial \mathbf{r}} \cdot \mathbf{a} + \frac{1}{2} \frac{\partial^2 \mathbf{S}(\mathbf{r})}{\partial \mathbf{r}^2} \cdot \mathbf{a}^2 + \dots, \quad (14)$$

where \mathbf{r} is the position of spin and $a = |\mathbf{a}|$ is the lattice constant, the equation of motion [Eq. (9)] can be written as

$$\frac{d}{dt} \mathbf{m}(\mathbf{r}) = \frac{2Jma^2}{\gamma} \mathbf{m}(\mathbf{r}) \times \nabla^2 \mathbf{m}(\mathbf{r}). \quad (15)$$

Here, the formula, $\mathbf{m} \times \nabla^2 \mathbf{m} = \operatorname{div}(\mathbf{m} \times \nabla \mathbf{m})$, yields

$$\frac{d}{dt} \mathbf{m}(\mathbf{r}) = -A\gamma \operatorname{div}(\mathbf{m} \times \nabla \mathbf{m}), \quad (16)$$

where $A = 2Ja^2/\gamma^2$ is the spin stiffness constant. By defining the current \mathbf{J}_s as

$$\mathbf{J}_s = A\gamma\mathbf{m}(\mathbf{r}) \times \nabla\mathbf{m}(\mathbf{r}), \quad (17)$$

it becomes clearer that the equation of motion [Eq. (16)] has the same form as the continuity equation [Eq. (5)] and expresses the conservation law of spin angular momentum in ferromagnets. \mathbf{J}_s defined by Eq. (17) is interpreted as a spin current carried by the exchange interaction, and is thereby called an exchange spin current [Fig. 1(c)].

D. Spin wave spin current

Next, consider the spin current carried by a spin wave [Fig. 1(d)]²². As a simple example, we focus on exchange spin waves propagating by exchange interaction. We assume the small amplitude oscillation of the magnetization $\mathbf{m}(\mathbf{r},t)$ about the fixed direction $\mathbf{m}_0 \parallel \mathbf{z}$ as

$$\mathbf{m}(\mathbf{r},t) = \mathbf{m}_0 + \mathbf{m}_x(\mathbf{r},t) + \mathbf{m}_y(\mathbf{r},t) \quad (|\mathbf{m}_0| \gg |\mathbf{m}_{x,y}|), \quad (18)$$

and we define

$$\psi(\mathbf{r},t) = m_x(\mathbf{r},t) + im_y(\mathbf{r},t), \quad (19)$$

$$\psi^*(\mathbf{r},t) = m_x(\mathbf{r},t) - im_y(\mathbf{r},t). \quad (20)$$

Using these expressions, the z component of the exchange spin current is rewritten as follows:

$$\mathbf{j}^{M_z} \propto \psi^*(\mathbf{r},t)\nabla\psi(\mathbf{r},t) - \psi(\mathbf{r},t)\nabla\psi^*(\mathbf{r},t). \quad (21)$$

By introducing magnons^{1,2}, the (exchange) spin current becomes

$$\mathbf{j}^{M_z} = \hbar \sum_{\mathbf{k}} \mathbf{v}_{\mathbf{k}} n_{\mathbf{k}}. \quad (22)$$

Here, $\mathbf{v}_{\mathbf{k}}$ is the group velocity of the spin wave, $n_{\mathbf{k}}$ is the distribution function of the magnons, and \mathbf{k} is the wave vector of spin waves. This formula means that when magnon population is asymmetric between \mathbf{k} and $-\mathbf{k}$, spin waves carry spin current.

III. SPIN-EXCHANGE COUPLING

The interaction of spin current and magnetization dynamics has been a central interest in spintronics for a long time^{1,23} and it is continuously being developed for better and lower power consumption device applications²⁴. The s-d exchange coupling is a key factor that controls spin-dependent transport and magnetization dynamics in ferromagnetic conductors and ferromagnetic/nonmagnetic interfaces owing to the ability that transfers angular momentum as well as energy between conduction spin and magnetization texture. These functionalities are at the heart of spin pumping^{1,25–27}, spin-transfer torque (STT)^{9–12}, and spinmotive force (SMF)^{16,28–36}. Various nonuniform magnetization textures, such as domain

walls (DWs) and skyrmions, are typical playgrounds for investigating STT and SMF in magnetic materials³⁷. Magnetic skyrmion also gives rise to the topological Hall effect (THE)^{38–42}. Such concepts realized in dynamical magnetization textures are routinely expressed by means of the emergent electromagnetic fields acting on electrons^{14,15,43}, whereby new device applications have been proposed so far^{44–46}.

This section focuses on the recent advances and perspectives on spin-exchange related phenomena including spin pumping, topological Hall effect, and emergent inductor.

A. Spin pumping

Spin pumping refers to the generation of a spin current, \mathbf{J}_s , from coherent magnetization \mathbf{M} precession in a magnet with metallic contact^{1,25–27} [Fig. 2(a)]. Here, the \mathbf{M} precession is driven by an applied microwave field, $\mathbf{h}(t)$, which satisfies the ferromagnetic resonance (FMR) condition. Under the FMR, the amplitude of the precessional magnetization motion is resonantly enhanced, and a part of its angular momenta is pumped out of the magnetic layer into a metal attached to the magnet due to the interfacial s-d exchange coupling. The generated (conduction-electron) spin current can be detected as a transverse electric voltage in the metal via the inverse spin Hall effect (ISHE)^{4–8} when the metal exhibits strong SOC [Fig. 2(a)].

Spin pumping has been intensively studied for a metallic ferromagnet $\text{Ni}_{81}\text{Fe}_{19}$ ^{4,5,7,27} and for a magnetic insulator $\text{Y}_3\text{Fe}_5\text{O}_{12}$ (YIG)^{22,49–51}. These magnetic materials exhibit high Curie temperatures, low Gilbert damping, and also small magnetic anisotropies, which makes their FMR frequencies to be \sim GHz range, accessible easily by experiments. In the past several years, various aspects of spin pumping have been reported with these materials. Some examples include spin pumping driven by parametric excitation⁵², a.c. spin pumping^{53–56}, and spin pumping induced by magnon polaritons^{57–59}, magnon polarons⁶⁰, and magnon-magnon hybrid systems^{61,62}.

In the following subsections, we discuss two recent topics related to spin pumping: Antiferromagnetic spin pumping and magnetic parametron based on a.c. spin pumping.

1. Antiferromagnetic spin pumping

In the emergent field of antiferromagnetic spintronics, spin pumping may offer promising opportunities to access the ultrafast magnetization dynamics^{63,64}. In contrast to ferromagnets, where the excitation frequency f of \mathbf{M} dynamics is governed by external (H) and anisotropy (H_A) fields (typically, \sim GHz frequencies), in antiferromagnetic (AF) materials, the dynamics depends on the combined effect of magnetic anisotropy (H_A) and the inter-sublattice exchange (H_E) fields, which leads to their excitation frequencies $f \sim (\gamma/2\pi)\sqrt{2H_E H_A}$ in the much higher (sub)terahertz range^{47,48,63,64}.

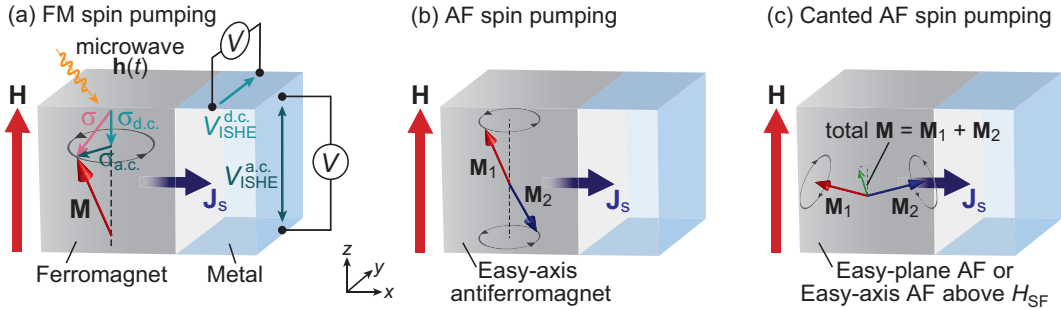


FIG. 2. Schematic illustrations of the (a) ferromagnetic (FM), (b) antiferromagnetic (AF), and (c) canted AF spin pumping. When an eigenmode of the magnetization \mathbf{M} dynamics is resonantly excited by the applied rf field $\mathbf{h}(t)$, a spin current, \mathbf{J}_s , is emitted from the magnet into the attached metal via the interfacial spin-exchange coupling. As shown in (a), the nonequilibrium spin polarization σ in spin pumping has d.c. ($\sigma_{\text{d.c.}}$) and a.c. ($\sigma_{\text{a.c.}}$) components: $\sigma = \sigma_{\text{d.c.}} + \sigma_{\text{a.c.}}$. When \mathbf{M} is oriented along the z direction by the external magnetic field \mathbf{H} , the d.c. polarization $\sigma_{\text{d.c.}}$ appears parallel to $\mathbf{H} \parallel \hat{\mathbf{z}}$, while the time-dependent $\sigma_{\text{a.c.}}$ rotates in the xy -plane. The d.c. (a.c.) ISHE voltage $V_{\text{ISHE}}^{\text{d.c.}}$ ($V_{\text{ISHE}}^{\text{a.c.}}$) is generated in the metal along the y (z) direction according to the relation $\mathbf{J}_s \times \sigma$, where $\mathbf{J}_s \parallel \hat{\mathbf{x}}^4$.

In 2020, Li *et al.*⁴⁷ and Vaidya *et al.*⁴⁸ demonstrated spin pumping from easy-axis antiferromagnets Cr_2O_3 and MnF_2 having the zero-field antiferromagnetic resonance (AFMR) frequency $f_0 \sim 0.16$ and 0.25 THz, respectively [depicted schematically in Fig. 2(b)]. In these antiferromagnets below the spin-flop field H_{SF} , there are two different AF spin-wave branches: high- f right-handed (RH) and low- f left-handed (LH) spin precessions with opposite polarizations⁴⁷ [Figs. 3(a)-3(d)]. Li *et al.*⁴⁷ performed AF spin pumping in Cr_2O_3 /(Pt or Ta) systems with a linearly polarized microwave at 0.240 THz and observed ISHE signals at the AFMR condition for the RH mode [Fig. 3(e)]. At a high temperature ($T \sim 100$ K), the polarity of the signal is consistent with that predicted from the spin polarization of the RH mode (σ_{RH}), which is same as that due to the quasi-ferromagnetic (QFM) spin-wave mode⁴⁷ [Figs. 3(c) and 3(d)]. Interestingly, with decreasing T , the sign reverses at around 45 K [Figs. 3(e) and 3(f)], which may be attributed to incoherent spin pumping (i.e., the spin Seebeck effect) from the LH mode (σ_{LH}) due to heating. Vaidya *et al.*⁴⁸ conducted AF spin pumping in MnF_2 /Pt samples with right- and left-circularly polarized microwaves that couple with high- f RH and low- f LH spin-wave modes in MnF_2 , respectively, at positive fields. They found that, when the right- (left-)circularly polarized microwaves are irradiated to the samples, an ISHE voltage with negative (positive) sign appears at 0.395 THz and 4.7 T (0.240 THz and 0.8 T) that satisfies the AFMR condition for the high- f RH (low- f LH) mode in MnF_2 [Figs. 3(g) and 3(h)]. This result agrees with the coherent spin-pumping scenario. They also observed spin-pumping signals at the resonance conditions for SF and QFM spin-wave modes [Figs. 3(g) and 3(h)], the characteristic of which is not yet fully understood and calls for further investigation from the viewpoint of both coherent and incoherent spin dynamics^{47,48}.

Spin pumping from different types of antiferromagnets has also been reported recently. In 2020, Moriyama *et al.*⁶⁵ reported AF spin pumping from NiO. Here, NiO is an easy-plane antiferromagnet with the Néel temperature (T_N) of 523

K and shows two linearly polarized magnon modes governed by two different anisotropies⁶⁶. They measured cw-THz wave transmission spectra through NiO-(Pt or Pd) granular systems at ~ 1 THz corresponding to the high- f AFMR mode in NiO arising from the hard axis anisotropy and found that the spectra linewidths for NiO-(Pt or Pd) are broader than that without Pt or Pd, indicating enhanced AF damping caused by spin pumping⁶⁵. Soon after, Qiu *et al.*⁶⁷ reported THz emission spectroscopy for NiO films covered by Pt or W films and showed ultrafast spin-current generation at zero external field and at room temperature, where a second-order nonlinear optical process in the NiO layer may play an important role. In 2021, Boventer *et al.*⁶⁸ and Wang *et al.*⁶⁹ independently reported spin pumping from a canted easy-plane antiferromagnet $\alpha\text{-Fe}_2\text{O}_3$ with metallic contacts (Pt or W), depicted schematically in Fig. 2(c). Above its Morin transition temperature ($T_M \sim 263$ K), the Fe^{3+} spins in $\alpha\text{-Fe}_2\text{O}_3$ lie in the basal (easy) plane of the corundum lattice and stack antiferromagnetically along the c axis⁶⁹. Here, $\alpha\text{-Fe}_2\text{O}_3$ exhibits the bulk Dzyaloshinskii–Moriya interaction, which cant the two AF sublattice moments slightly, giving rise to an RH elliptical precessional mode of the net moment in the range of 10 GHz [Fig. 3(d)], much lower than its high- f mode associated with out-of-plane oscillation of the Néel vector (0.17 THz). Boventer *et al.*⁶⁸ and Wang *et al.*⁶⁹ developed the general framework for the spin pumping from this low- f mode and experimentally demonstrated the concept through the ISHE measurements.

2. Towards stochastic computing based on a.c. spin pumping

Electric read-out of spin information based on spin pumping and ISHE may provide a potential route for future computational technologies. In 2021, Makiuchi *et al.*⁷⁰ realized a parametric oscillator based on a YIG disk that acts as a “magnetic parametron”, a nonlinear magnetic oscillator whose precessional phases are discretized into Ising-like

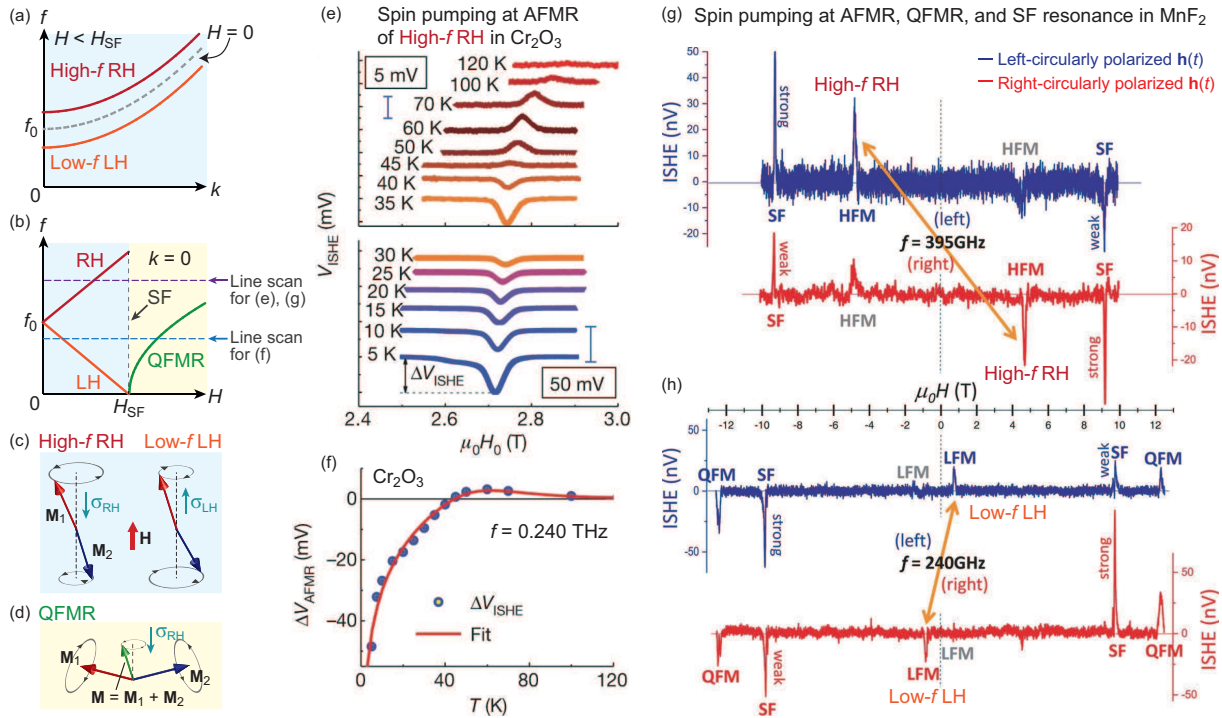


FIG. 3. (a) Schematic illustrations of the AF spin-wave dispersion relations for an easy-axis antiferromagnet below the spin-flop field H_{SF} . There are two AF branches: high- f right-handed (RH) and low- f left-handed (LH) spin-wave modes with opposite spin polarizations σ_{RH} and σ_{LH} , respectively, which are degenerate at f_0 for $H = 0$ ($f_0 \sim 0.16$ THz for Cr_2O_3 ⁴⁷ and 0.25 THz for MnF_2 ⁴⁸). (b) Resonance frequency versus H for $k = 0$ (k : wavenumber). For $H > H_{\text{SF}}$, a quasi-ferromagnetic resonance (QFMR) mode shows up. (c),(d) Schematic illustrations of (c) high- f RH and low- f LF spin-wave modes for $H < H_{\text{SF}}$ and (d) QFMR mode for $H > H_{\text{SF}}$. (e),(f) ISHE voltage signals at the AFMR of high- f RH mode versus (e) external H and (f) temperature T , when a linearly-polarized microwave at $f = 0.240$ THz is applied to a Cr_2O_3 /(Pt-Ta) sample⁴⁷. (g),(h) ISHE voltage signals versus H when a circularly-polarized microwave at (g) $f = 0.395$ and (h) 0.240 THz is applied to MnF_2 /Pt samples, which excites the (g) high- f RH and SF and (h) low- f LH, SF, and QFMR modes in MnF_2 , respectively⁴⁸. (e),(f) Reproduced with permission from Li *et al.*, Nature **578**, 70–74 (2020). Copyright 2020 Springer Nature Limited. (g),(h) Reproduced with permission from Vaidya *et al.*, Science **368**, 160–165 (2020). Copyright 2020 American Association for the Advancement of Science (AAAS).

0 or π relative to the applied microwave phase (Fig. 4). In their experiment⁷⁰, the binary phase of magnetization \mathbf{M} precession (with angular frequency ω) is realized by parallel parametric pumping in the YIG disk with shape magnetic anisotropy; when a 2ω microwave for the parametric excitation is turned on, one of the energetically-degenerated phase states are spontaneously selected [Figs. 4(b) and 4(c)]. The phase information can be electrically read out through a.c. spin pumping and ISHE measurements [see Fig. 2(a)] in a Pt film attached to the YIG disk at room temperature. Makiiuchi *et al.*⁷⁰ showed that the phase states undergo transition between stable and stochastic regimes by increasing the excitation power [Fig. 4(d)]. In the latter regime, they further demonstrated that the occurrence probability of each state can be tuned with additional microwaves, showing its potential application as a “probabilistic bit (p-bit)” in stochastic computation. By combining the above experimental technique with that established in quantum optics, Hioki *et al.*⁷¹ demonstrated the state tomography for magnetization dynamics and obtained a density matrix and Wigner function realized in a magnetic parametron, which shows a mixed state

composed of two coherent states [Figs. 4(e)-4(g)]. Shimizu *et al.*⁷² numerically studied the spin dynamics in a magnetic parametron based on a master equation and found that amplitude squeezed states can be formed under strongly biased microwaves. More recently, Elyasi *et al.*⁷³ theoretically showed that there are three dynamical phases in the dynamics of the magnetic parametron: a stable Ising spin, telegraph noise of thermally activated switching, and an intermediate regime that at lower temperatures is quantum correlated with significant distillable magnon entanglement. Their finding further expands the scope of the application of magnetic parametron as a quantum information processor⁷⁴.

B. Topological Hall torque

Electrical manipulation of magnetization is important for establishing next-generation magnetic storage such as magnetoresistive random access memory (MRAM). To this end, electrically induced torques exerting on magnetic textures has been considered as a working principle. Two types of such

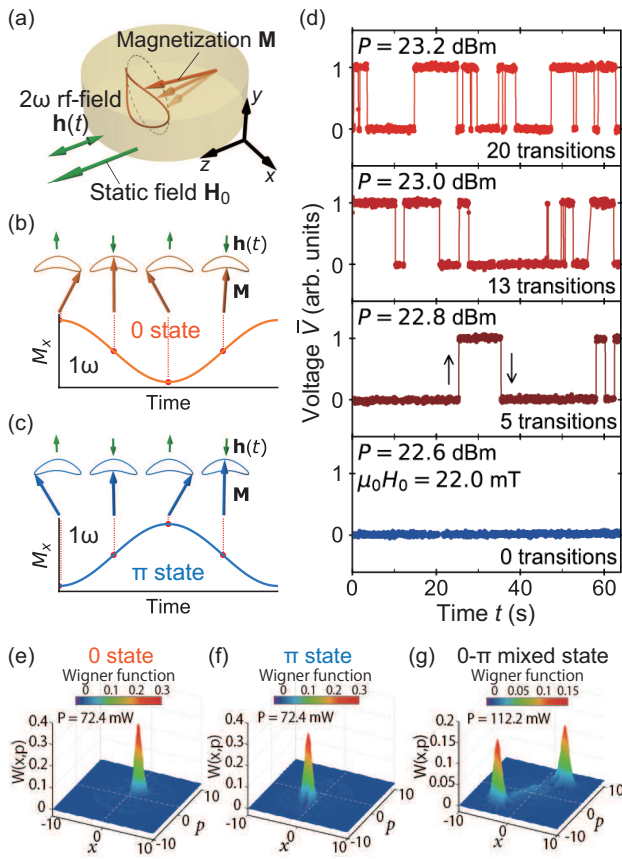


FIG. 4. (a) A schematic illustration of the parametrically excited magnetization \mathbf{M} precession in a YIG disk⁷⁰. (b),(c) Time evolution of M_x (with angular frequency ω) for the (b) 0-phase and (c) π -phase state that is a relative phase between M_x and the input 2ω microwave field $\mathbf{h}(t)$, respectively⁷⁰. (d) The normalized ISHE voltage \bar{V} induced by a.c. spin pumping versus time at selected values of microwave power P for a YIG/Pt disk⁷⁰. (e),(f),(g) Reconstructed Wigner function for the (e) 0-phase, (f) π -phase, and (g) 0- π phase mixed state through magnetization state tomography⁷¹. (a)-(d) Reproduced with permission from Makiuchi *et al.*, *Appl. Phys. Lett.* **118**, 022402 (2021). Copyright 2021 AIP Publishing LLC. (e)-(g) Reproduced with permission from Hioki *et al.*, *Phys. Rev. B* **104**, L100419 (2021). Copyright 2021 American Physical Society.

torques were identified: STT^{9,11,12} [Fig. 5(a)] and spin-orbit torque (SOT)⁷⁵⁻⁸⁰, aiming at a high-speed and energy-efficient writing scheme for MRAM. The effects are proportional to charge-to-spin conversion ratio, and thus highly spin-charge coupled systems are pursued for energy-efficient DW motion. However, they face a physical limit of charge-to-spin conversion ratio, which is a fundamental obstacle in those conventional mechanisms. To circumvent this problem, the use of topological physics, particularly, Weyl electrons emerging around Weyl points (WPs), can be a solution since electrons acquire the highly efficient charge-to-spin conversion thanks to the large fictitious magnetic field (Berry curvature) and spin-momentum locking (SML).

The momentum-space Berry curvature leads to the anomalous velocity transverse to the applied electric field, which is

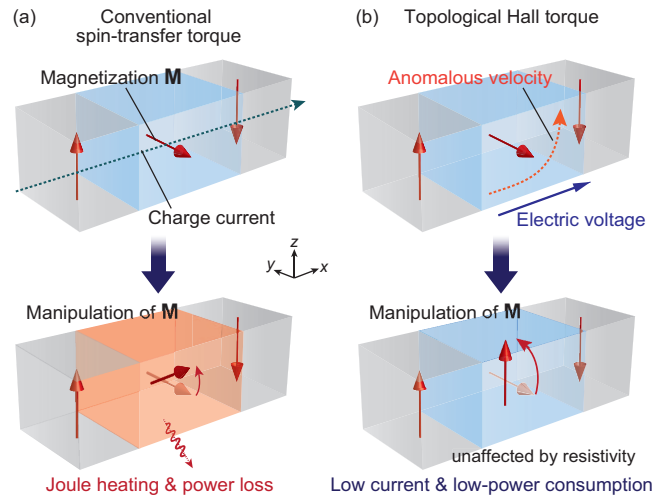


FIG. 5. Schematic illustrations of the (a) conventional spin-transfer torque (STT) exerted on a magnetic texture by a dissipative charge current and (b) topological Hall torque (THT) emerging via nondissipative anomalous Hall current by applying an electric voltage.

the origin of the intrinsic anomalous Hall effect (AHE)⁸¹⁻⁸⁵. In the vicinity of band inversion point associated with the strong SOC on the surface of topological insulators (TIs)⁸⁶⁻⁸⁹ and in Weyl semimetals (WSMs)⁹⁰⁻⁹⁸, the Berry curvature becomes significant and yields a large anomalous Hall conductivity. Relying on the strong SOC, the electrically induced torques was studied within particular models of TIs⁹⁹⁻¹⁰⁶ and WSMs¹⁰⁷⁻¹⁰⁹. In the recent study, a classification of the contributions to the torques based on the semiclassical (Boltzmann) formalism has been established¹¹⁰, revealing that the emergence of intrinsic torques driven by the anomalous velocity via SML. In comparison with the the conventional STT^{9,11,12} [Fig. 5(a)] and SOT⁷⁵⁻⁸⁰ induced by transport current, the intrinsic torques are robust against disorder or thermal fluctuation. The inverse spin-galvanic effect was proposed at the surface states of topological insulators attached to ferromagnets⁹⁹ and has been demonstrated experimentally¹¹¹. Even in bulk crystals without breaking of inversion symmetry by surfaces or interfaces, an intrinsic torque is generated by the coupling of momentum-space Berry curvature with real-space magnetic textures¹¹⁰, which was called the “topological Hall torque (THT)” [Fig. 5(b)].

The structure of the THT is formally compatible with the field-like STT albeit it does not rely on the transport spin current flowing through magnetic textures such as DWs. Recently, an interaction between a DW and Weyl electrons has been investigated in a ferromagnetic oxide SrRuO_3 ¹¹², which has many WPs near Fermi level. Although the current density required for the DW motion in SrRuO_3 is more than one order of magnitude lower than that in metallic systems^{113,114}, its mechanisms have been unsolved until Ref. [112]. When a current is applied across the DW, an effective magnetic field H_{eff} is exerted on the DW. The ratio of H_{eff} per current density is “over one order of magnitude higher (more efficient)” than that originating from conventional STT and SOT reported

so far. Within a framework of THT, by inserting the values typical in SrRuO_3 , the magnitude of $\mu_0 H_{\text{eff}}/J$ to be $10 - 12 \text{ Tm}^2/\text{A}$, which formally corresponds to the nonadiabaticity parameter $\beta_{\text{THT}} \simeq 2$ and matches the measured value.

While effects of Weyl electrons appear in a wide variety of phenomena such as, magnetotransport⁹⁰⁻⁹⁸, spin wave¹¹⁵, quantum phenomena, and thermoelectric phenomena, the findings in Ref.[112] add DW dynamics to that catalog and pave the way for an energy-efficient scheme for electrical manipulation of magnetization, which is essential in the operation of next-generation magnetic storage devices. Prominently, the mechanism reported in Ref. [110] is not limited to the special class of Weyl semimetals but appears in a ferromagnetic metal with WPs, which is more general material. The new torque mechanism, THT, therefore, offers applications of topological physics, one of the major topics in current solid-state physics, to spintronics.

C. Emergent inductor

Inductors are one of the basic components in electric circuits realizing functions such as voltage transformation, noise filtering, switching, and so on. The working principle relies on the classical electromagnetics: a conducting coil stores the energy in a magnetic field when an electric current flows through it, leading to the induction of an electromotive force that opposes the change in the current. An inductance of a solenoid coil is given by $L = \mu n^2 l A$, where μ , n , l , and A are the permeability, turn density, length, and cross-section of the coil, respectively. This relation indicates that the magnitude of the inductance scales with the size of the solenoid, which limits downsizing inductors equipped within microcircuits.

Because the SMF is the spin version of Faraday's law of induction one can envisage the spin-extension of inductor operation in magnetic nanostructures. This was actually invented by a theoretical proposal of the so-called "emergent inductor" using a spiral magnet⁴⁶. When an electric current flows in a spiral magnet, it stores the energy in the spiral structure formed by the local magnetization via its exchange coupling with conduction electrons. In terms of the Berry phase formalism, the emergent inductance can be thought of as an extension of the dynamical Aharonov-Bohm effect to a spiral magnet, where the electromagnetic potential is replaced by a spin-dependent Berry connection generated by the spatial variation of the magnetization^{16,28,29}. Focusing on the adiabatic processes of STT and SMF, the inductance originating from spiral dynamics can be expressed as the following simple formula,

$$L = \left(\frac{p\hbar q}{2e\sqrt{K}} \right)^2 \frac{l}{A}, \quad (23)$$

where p is the spin polarization, \hbar is the Dirac constant, q is the spiral wave number, e is the elementary charge, K is the magnetic hard axis anisotropy constant, l is the length and A is the cross-sectional area of the spiral magnet. A prominent feature of emergent inductors is its size dependence of

the magnitude of inductance. Contrary to the coil inductance that is proportional to the coil cross section area A ($L \propto A$), the emergent inductance is inversely proportional to the area that the current passing through ($L \propto A^{-1}$). This property opens an innovative avenue for downsizing inductor elements.

Soon after the theoretical proposal, the concept was experimentally demonstrated in a centrosymmetric helical magnet $\text{Gd}_3\text{Ru}_4\text{Al}_{12}$ ¹¹⁶. More recent theoretical works have shown that two excitation modes of a spiral magnetic texture, namely its translational displacement and rotation of the spiral plane, contribute to emergent inductance with opposite signs^{117,118}. This may explain the negative inductance observed in the experiment¹¹⁶, whereas the original theory, which takes only into account the rotational excitation, predicted positive⁴⁶. Experimentally, a room temperature observation of emergent inductance has been achieved in YMn_6Sn_6 ¹¹⁹, while in Ref. 116 the temperature had to be as low as below $\sim 20 \text{ K}$ with $\text{Gd}_3\text{Ru}_4\text{Al}_{12}$ used. The discovery of emergent inductance has reopened the textbook of electronics and we are at the beginning of a new chapter exploring quantum mechanical mechanisms of inductance.

The concept of the emergent inductor is not limited to the original spiral dynamics. In fact, a novel inductance of SOC origin, was proposed¹²⁰ where a SOC stores the energy in itself as well as mediates the energy conversion with the electric energy. The spin-orbit inductance results from the time derivative of Aharonov-Casher phase¹²¹ in magnetic materials, where the Berry connection originating from SOCs depends on the electron's momentum as well as spin. As already shown in Ref. 117, effects of a Rashba-type SOC play significant roles in a spiral-based emergent inductor. The spin-orbit inductance can be formulated based on a dynamical spin Berry phase acquired by an electron moving in arbitrary magnetic textures in the presence of SOCs in a general form.

$$L_{ij} = \frac{pm_e}{e} \frac{l_i}{A} \sum_k g_{ik} \chi_{\omega}^{kj}, \quad (24)$$

where m_e is the electron mass, l_i is the dimension of the sample in the x_i direction, A is the cross sectional area normal to the electric current, g_{ij} is the general SOC, and χ_{ω}^{ij} is the magnetic susceptibility tensor with respect to current-induced torques. A particular interest is on exploring spin-orbit inductance with spatially uniform magnetization, where the other inductance mechanisms are ruled out. With the ferromagnetic resonance frequency ω_R defined by $\omega_R \propto K$ (K is the hard axis anisotropy constant), the dynamical susceptibility for $\omega \ll \omega_R$ can be approximated by $(\chi_{\omega}^{xx}, \chi_{\omega}^{yy}) \simeq -\frac{pm_e}{2eK} (g_{xx}, g_{yy})$. In this low frequency regime, the inductances Eq.(24) can be thus approximated by

$$L_{xx} = \left(\frac{pm_e}{\sqrt{2}e} \right)^2 \frac{l_x}{A} \frac{g_{xx}^2 + g_{yy}^2}{K}, \quad (25)$$

$$L_{yy} = \left(\frac{pm_e}{\sqrt{2}e} \right)^2 \frac{l_y}{A} \frac{g_{yx}g_{xx} + g_{yy}g_{xy}}{K}. \quad (26)$$

Note that spin-orbit inductance appears in both the longitudinal and transverse (Hall) directions with respect to a current and they are second order of the SOC constants g_{ij} .

From technological perspectives, we compare classical, spiral-based, and spin-orbit inductances as follows. The classical inductance scales with the size of the coil, making it highly challenging to miniaturize an inductor and the devices containing ones. The spiral-based emergent inductance, originating from the quantum-mechanical exchange coupling effect, is free from the undesirable system-size dependence, being indeed inversely proportional to the system's cross sectional area (normal to the electric current direction)⁴⁶. In Ref. 116, an emergent inductance has been reported comparable in its magnitude to that of a commercial one (~ 400 nH), but in a volume about a million times smaller. While the emergent inductance has broken a hurdle for manufacturing smaller inductors with larger effects, it confronts its own problem, which is the limitation in the operating frequency. The previous experiments successfully observed the emergent inductance only up to the frequencies of sub-megahertz¹¹⁹ and megahertz¹¹⁶, because a spiral magnetic structure cannot respond collectively and robustly to electric currents with higher frequencies. The spin-orbit inductance resolves the two issues, regarding miniaturization and the operating frequency, simultaneously. As seen in Eq. (24), smaller the cross sectional area A , larger the spin-orbit inductance, as with the case for the spiral-based emergent inductance. The spin-orbit inductance with spatially uniform magnetization also provides the nearly frequency independent real parts except at the vicinity of the resonance frequency, which is typically $\sim 1\text{-}10$ GHz. Potential candidate systems for experimental observation of the spin-orbit inductance include heavy metal/ferromagnet heterostructures, where a Rashba SOC arises due to the structural inversion asymmetry. Those systems have been extensively studied in spintronics for use of non-volatile memory devices⁷⁷⁻⁸⁰. Adopting here $g = 10^{-10}$ eV·m/ \hbar ⁷⁷, and employing some typical values for the other relevant material parameters as $K \sim 10^5$ J/m³, $p \sim 0.5$, and the bare electron mass for m_e , L_{xx} in Eq. (25) is estimated as $\sim 10^{-18} \times (l_x/A)$ H. Assuming the sample dimensions of $(l_x, l_y, l_z) = (0.1\text{mm}, 100\text{nm}, 10\text{nm})$, we thus arrive at an estimation $L_{xx} \sim 100$ nH. In the context of the conventional spintronics applications, larger K has been mostly pursued for better thermal stability of the magnetic configuration²⁴. For a larger spin-orbit inductance, in contrast, smaller K is rather preferred, see Eqs. (23)-(26), while it also leads to a lower resonance frequency. It is desired to systematically conduct experimental and material research in the future to achieve optimal conditions for the spin-orbit inductance, i.e., simultaneous realization of larger g_{ij} , smaller A , and the right magnitude of K depending on the purpose.

IV. SPIN-HEAT COUPLING

We now extend our discussion to the interaction/interconversion of spins with heat, lattice vibrations, and charge current. Starting with a brief introduction and advances of spin-lattice coupling, we here address the recent progress and perspectives on the spin Seebeck and Peltier effects, two representative spin-heat coupling phenomena.

A. Spin-lattice coupling

Spin-lattice coupling is a fundamental mechanism of spin-heat coupling and responsible for various phenomena that change both static and dynamical magnetization/lattice states, such as magnetostriction, magneto-volume effect (MVE) [Fig. 6(a)], and magnon-phonon interaction (leading to magnon-phonon thermalization). The mechanism can be classified into two-ion and single-ion types¹²²⁻¹²⁴. The former one arises due to the change of the exchange interaction (J) between magnetic atoms (or ions) when their distances are modulated by lattice vibrations, while the latter one due to the strain-induced change of the magnetic anisotropy, or spin-orbit interaction¹²²⁻¹²⁴.

Recently, spin-lattice coupling has renewed attention in spintronics. By the single-ion type interaction, magnons and phonons, in the vicinity of the crossings of their dispersion relations, are hybridized into quasiparticles called “magnon polarons” that share mixed magnonic and phononic characters¹²⁶⁻¹²⁹. Magnon polarons can convey spin information with velocities close to those of phonons, much faster than the magnon velocities in the dipolar regime^{127,130}. Besides, thanks to the long-lived phononic constituent, magnon polarons may have longer lifetimes than pure magnons, and can enhance the spin-current related phenomena, such as spin pumping⁶⁰ (Sec. III A) and the spin Seebeck/Peltier effects^{128,129,131} (Secs. IV B and IV C). Magnon-phonon interconversion have also been detected through Brillouin light scattering¹³², FMR¹³³, and spatio-temporal imaging¹³⁴ spectroscopy, which may open a new avenue for empowering information transfer with magnon polarons in quantum transduction devices^{135,136}.

To further utilize spin-lattice coupling in spintronics, spin-current injection into a large magnetostrictive material may offer a unique opportunity. In 2022, Arisawa *et al.* showed that volume of a magnet can be manipulated by injecting a spin current: a spin-current volume effect (SVE) [Fig. 6(b)]¹²⁵. They observed that the thickness of thin films of ferromagnetic Tb_{0.3}Dy_{0.7}Fe₂ exhibiting strong spin-lattice coupling changes by a spin current induced by the spin Hall effect (SHE) of the attached Pt or W films [Figs. 6(c) and 6(d)]. Theoretical calculation revealed that modulation of magnetization fluctuation due to the spin-current injection play an essential role¹²⁵. The SVE enables direct mechanical actuation of a magnetostrictive thin film by using a spin current and may provide a promising approach to explore spintronic phenomena driven by spin-lattice coupling.

B. Spin Seebeck effect

1. Spin Seebeck effects driven by ferro- and antiferro-magnons

The spin Seebeck effect (SSE)¹³⁷⁻¹³⁹ refers to the generation of a spin current, \mathbf{J}_s , as a result of a temperature gradient, ∇T , in magnetic materials. It is well established for magnetic insulators with metallic contacts, at which a

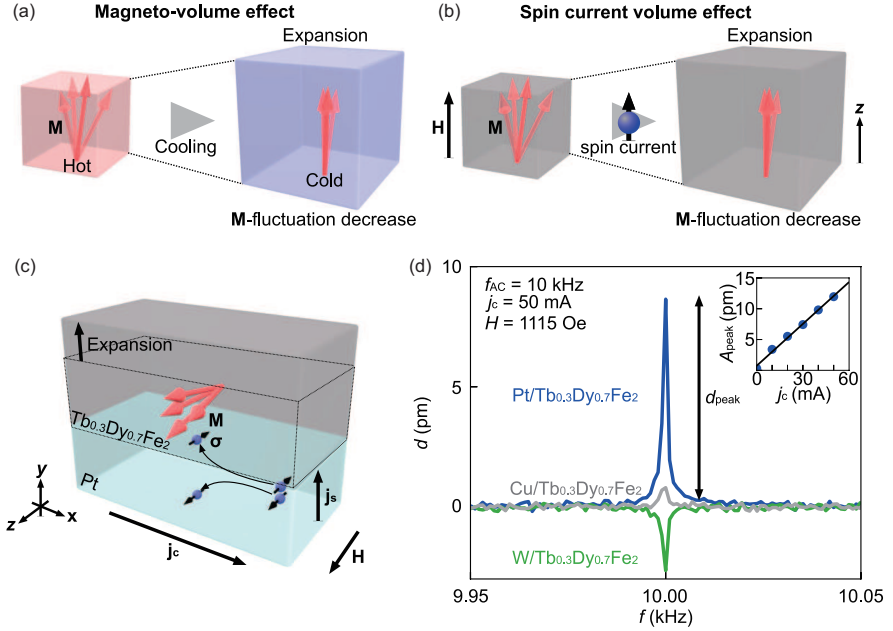


FIG. 6. (a) A schematic illustration of the magneto-volume effect (MVE). A ferromagnet expands (shrinks) via the spin-lattice coupling when spin fluctuation in the magnet decreases (increases) due to the magnetic-field \mathbf{H} application or temperature modulation¹²⁵. (b) A schematic illustration of spin-current volume effect (SVE), where volume of a ferromagnet is tuned by spin-current injection¹²⁵. (c) A schematic illustration of SVE induced by the SHE in a Pt/Tb_{0.3}Dy_{0.7}Fe₂ system¹²⁵. When a charge current, \mathbf{j}_c , is applied to the Pt film, a spin current, $\mathbf{j}_s \parallel \hat{\mathbf{y}}$ (with spin polarization $\sigma \parallel \hat{\mathbf{z}}$), is injected into the Tb_{0.3}Dy_{0.7}Fe₂ film, and magnetization \mathbf{M} fluctuation in the Tb_{0.3}Dy_{0.7}Fe₂ film decreases. This causes the volume expansion via the spin-lattice coupling, which accompanies a thickness change of the Tb_{0.3}Dy_{0.7}Fe₂ film¹²⁵. (d) Mechanical vibrational spectrum (the signed amplitude of the vibration d) for (Pt, W, Cu)/Tb_{0.3}Dy_{0.7}Fe₂ samples measured with laser Doppler vibrometry. The inset shows the j_c dependence of the mechanical vibration amplitude A_{peak} at $H = 1530$ Oe¹²⁵. Reproduced from Arisawa *et al.*, Nat. Commun. **13**, 2440 (2022). Copyright 2022 Author(s), licensed under a Creative Commons Attribution (CC BY) license.

magnon spin current is converted into a conduction-electron spin current by the interfacial s-d exchange coupling and detected as an ISHE voltage^{140–144} [Fig. 7(a)]. In particular, the YIG/Pt heterostructure¹⁴⁵ has become a prototype system. The ferrimagnetic YIG exhibits the lowest magnetic damping, high Curie temperature ($T_C \sim 560$ K), and high resistivity owing to a large band gap^{50,146}, while Pt is a paramagnetic metal showing high ISHE efficiency^{147,148}, which are ideal for SSE measurements. A number of experiments have been conducted with use of YIG and YIG/Pt systems to reveal the physics behind SSEs. Reports include temperature^{149–153}, magnetic field^{128,150–152,154–157}, length-scale (thickness)^{150–152,157–161}, structural^{162,163}, and time^{164–169} dependence measurements, separation with other (thermo)electric and spin-current effects^{170–178}, quantitative estimation of SSE thermoelectric coefficient^{179–181}, neutron scattering experiments to determine magnon dispersions for unraveling SSE features^{182–185}, evaluation of a magnon temperature and chemical potential^{144,186–189}, and so on.

The SSE provide a much easier way to generate a spin current through AF spin dynamics compared to coherent spin pumping which needs microwave instruments compatible with a subterahertz range^{47,48}. Since 2015, AF SSEs have been reported for various materials including Cr₂O₃^{47,190–195}, MnF₂¹⁹⁶, FeF₂¹⁹⁷, α –

Fe₂O₃^{193,198,199}, NiO^{200–203}, α -Cu₂V₂O₇²⁰⁴, MnPS₃^{205,206}, SrFeO₃²⁰⁷, SrMnO₃²⁰⁸, YFeO₃²⁰⁹, LaFeO₃²¹⁰, LuFeO₃²¹¹, DyFeO₃²¹², and electrically-switchable BiFeO₃²¹³, showing versatility of the SSE to investigate AF spin dynamics. There is, however, still debate on the H response for easy-axis antiferromagnets below H_{SF} . Seki *et al.*¹⁹⁰ did not observe any detectable signal in Cr₂O₃/Pt, while Wu *et al.*¹⁹⁶ observed a ferromagnetic (positive) sign¹⁷³. Recently, Li *et al.*^{47,192,193} reported a negative sign for Cr₂O₃/Pt and α -Fe₂O₃/Pt in its easy-axis AF phase ($T < T_M$), which is consistent with the spin polarization carried by the low- f LH mode [Figs. 3(a)–3(c)]. The magnon-polaron SSE anomalies observed in Cr₂O₃/Pt corroborate the scenario¹⁹². Li *et al.*^{47,193} further showed that the SSE sign for $H < H_{\text{SF}}$ changes from negative to positive when the surface of Cr₂O₃ is etched before Pt deposition. The result may be interpreted in terms of the appearance of uncompensated magnetic moments at the interface that contribute to the positive ferromagnetic-like SSE signal through modification of the interfacial spin-mixing conductance or generation of an additional spin current^{47,193}. The sign of AF SSE for $H < H_{\text{SF}}$ is also a subject of theoretical investigations^{214–217}. The interfacial and bulk magnon transport theories for AF SSEs predict the negative sign due to greater thermal occupation of the low- f LH mode^{214,216}. By contrast, the Landau-Ginzburg theory²¹⁵ near T_N concludes

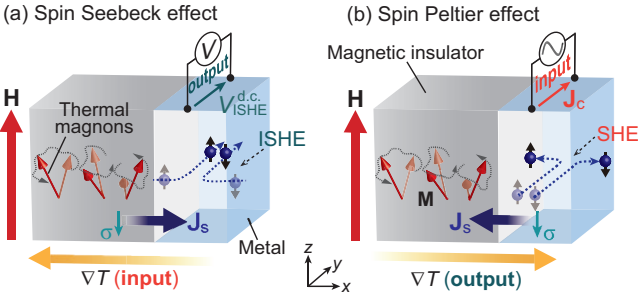


FIG. 7. (a),(b) Schematic illustrations of the (a) SSE and (b) SPE in a magnetic insulator with metal contact. (a) For the SSE, an applied temperature gradient, ∇T ($\parallel \hat{x}$), excites a magnon flow, which at the interface to the metal becomes a conduction-electron spin current, $J_s \parallel \hat{x}$ (with spin polarization $\sigma \parallel H \parallel \hat{z}$), and is converted into a transverse voltage by the ISHE according to the relation $J_s \times \sigma$. (b) For the SPE, an applied charge current, J_c ($\parallel \hat{y}$), generates a conduction-electron spin current, $J_s \parallel \hat{x}$ (with spin polarization $\sigma \parallel \hat{z}$), by the SHE, which at the interface to the magnet is converted into a magnon flow. Due to the energy conservation, this process accompanies a heat transfer between the electron and magnon systems, leading to a measurable temperature difference between the metal and magnet.

to have the same sign as ferromagnets. Further experimental and theoretical studies would therefore be desirable to elucidate the mechanisms behind the AF SSEs. Very recently, Yamamoto *et al.*²¹⁷ theoretically addressed the sign issue and showed that the negative (positive) sign appears for $H < H_{SF}$ under the condition that the interfacial coupling between the conduction-electron spins s and the Néel order n (net magnetization m) of the AF layer dominates the interfacial spin-current generation.

Van der Waals two-dimensional (2D) materials may also be an intriguing platform for studying SSEs. Ito *et al.*²¹⁸ studied the SSE in quasi-2D layered ferromagnets $\text{Cr}_2\text{Si}_2\text{Te}_6$ ($T_C \sim 31$ K) and $\text{Cr}_2\text{Ge}_2\text{Te}_6$ ($T_C \sim 65$ K) with Pt contacts. Here, these 2D materials show in-plane short-range ferromagnetic correlations which survive up to at least 300 K (for $\text{Cr}_2\text{Si}_2\text{Te}_6$), whereas out-of-plane correlations disappear slightly above T_C ²¹⁹. The SSE in these systems turned out to persist above T_C , which may be attributed to exchange-dominated interlayer transport of in-plane paramagnetic moments reinforced by short-range ferromagnetic correlations and strong Zeeman effects²¹⁸. Magnon transport in 2D magnets such as antiferromagnetic MnPS_3 ^{205,206} and ferromagnetic CrBr_3 ²²⁰ has also been investigated via nonlocal SSEs. In 2020, Lee *et al.*²²¹ showed that, when a monolayer WSe_2 inserted between Pt and YIG layers, the SSE is enhanced by a factor of ~ 5 compared to that in a Pt/YIG system, which may offer a new opportunity on the SSE research with 2D transition dichalcogenide materials.

In the following of this section, we will give an overview and perspective about the selected recent topics in SSE research: SSEs driven by magnon polarons, quantum spins, and nuclear spins. We also briefly discuss the reciprocal of SSE: the spin Peltier effect.

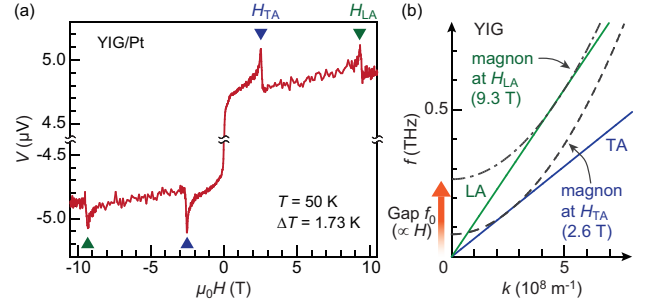


FIG. 8. (a) H dependence of longitudinal SSE voltage V for a YIG-film/Pt system at the temperature $T = 50$ K under the temperature difference $\Delta T = 1.73$ K¹²⁸. (b) Magnon, TA-, and LA-phonon dispersion relations for YIG at the touching field $H = H_{\text{TA}}$ ($= 2.6$ T) and H_{LA} ($= 9.3$ T). The magnon gap f_0 can be tuned with the external H due to the Zeeman interaction ($f_0 \propto \gamma\mu_0H$). (a) Reproduced from Kikkawa *et al.*, Phys. Rev. Lett. **117**, 207203 (2016). Copyright 2016 American Physical Society.

2. Magnon-polaron spin Seebeck effect

Recent experiments have revealed that small saw-tooth peak structures appear in magnetic field-dependent SSE voltages [see Fig. 8(a)] that shows the H dependence of SSE for a YIG/Pt bilayer¹²⁸, which is explained in terms of excitations of magnon polarons having both magnonic and phononic constituents^{128,129}. The SSE anomalies show up when the magnon dispersion shifts upward with external H such that the phonon dispersion curves become tangential [Fig. 8(b)]. Under these “touching” conditions, the magnon and phonon modes can be coupled over the largest frequency window in momentum space, so the effect of magnon-polaron formation in magnonic spin transport is maximal. If the phonon lifetime is longer than the magnonic one, magnon polarons will have a longer lifetime than pure magnons, and can thus enhance the SSE^{128,129}. Indeed, the SSE anomalies are well reproduced by solutions of a Boltzmann equation for the strongly coupled magnon-phonon systems, in which the magnon-phonon lifetime difference is taken into consideration^{128,129}. So far, the magnon-polaron anomalies in SSEs have been reported in ferrimagnetic YIG^{128,139,222–224}, $\text{Bi}_x\text{Y}_{3-x}\text{Fe}_5\text{O}_{12}$ ²²⁵, Fe_3O_4 ²²⁶, NiFe_2O_4 ²²⁷, $\text{Ni}_{0.65}\text{Zn}_{0.35}\text{Al}_{0.8}\text{Fe}_{1.2}\text{O}_4$ ²²⁸, (partially) compensated ferrimagnetic $\text{Lu}_2\text{Bi}_1\text{Fe}_4\text{Ga}_1\text{O}_{12}$ ²²⁹ and $\text{Gd}_3\text{Fe}_5\text{O}_{12}$ ²³⁰, and antiferromagnetic Cr_2O_3 ¹⁹². These works demonstrate the power of SSEs to reveal spectroscopic information on the spin dynamics in various magnetic insulators.

The formation of magnon polarons is predicted to affect magnonic spin and thermal conductivities¹²⁹ and also, in a non-local configuration, to appear as a Fulde-Ferrell-Larkin-Ovchinnikov (FFLO)-like oscillatory voltage as a function of injector-detector distance²³¹, which await experimental discovery. Another interesting challenge would be the elucidation of anisotropic magnon-polaron transport recently found through the longitudinal and nonlocal SSE measurements²²⁵. It is worthwhile to mention that under sufficiently strong magnon-magnon and phonon-phonon scatterings, the coher-

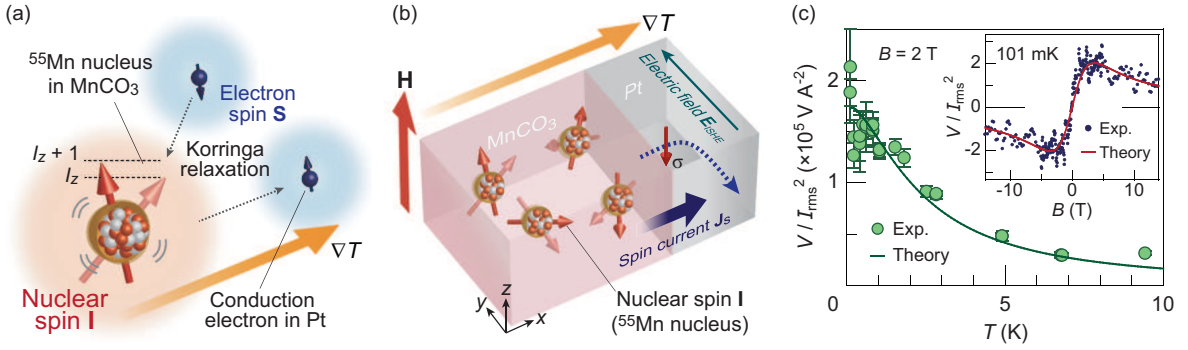


FIG. 9. (a) A schematic illustration of the nuclear SSE induced by the Korringa relaxation process, the spin-conserving flip-flop scattering between a nuclear spin, \mathbf{I} , of ^{55}Mn in MnCO_3 and an electron spin, \mathbf{S} , in Pt via the interfacial hyperfine interaction. (b) A schematic illustration of the nuclear SSE in a MnCO_3 /Pt structure. (c) T dependence of the nuclear SSE voltage V (normalized by the applied heat power $\propto I_{\text{rms}}^2$) at $B = 2 \text{ T}$. The inset shows the B dependence of V/I_{rms}^2 at $T = 101 \text{ mK}$. Theoretical results for the nuclear SSE are also plotted with solid curves. (a)-(c) Reproduced from Kikkawa *et al.*, *Nat. Commun.* **12**, 4356 (2021). Copyright 2021 Author(s), licensed under a Creative Commons Attribution (CC BY) license.

ent magnon-polaron picture may become invalid. Schmidt *et al.*²³² formulated a Boltzmann transport theory in such a parameter regime and showed that similar anomalies in the SSE manifest through the “phonon drag” process at the touching fields.

3. Quantum-spin Seebeck effect

Collective excitations of localized spins are not limited to spin waves, and more exotic excitations are known to exist in quantum spin liquids (QSLs), but have not yet been discussed in the context of spintronics until recently^{233–235}. In QSLs, localized spins do not exhibit long-range order but maintain spin correlation due to the quantum fluctuation reinforced by low dimensionality or frustration²³⁴. A well established example is a one-dimensional (1D) QSL in which a spin-1/2 chain coupled via AF interaction and exhibits a gapless elementary excitation, called a “spinon”. In 2017, Hirobe *et al.*²³³ demonstrated the spinon SSE in Sr_2CuO_3 having 1D Cu^{2+} spin ($S = 1/2$) with large nearest-neighbor exchange coupling ($\sim 2000 \text{ K}$). The observed spinon SSE is characterized by two features: the non-saturating H -response and negative sign. The former one is ascribable to the robust gapless feature of spinons with the large exchange coupling, while the latter mainly to the singlet correlation in the spin chains^{233,234}. The demonstration may serve as a bridge between spintronics and quantum-spin communities which have been developed independently for many years. Recently, Chen *et al.*²³⁵ expanded the concept of the quantum-spin Seebeck effect to a gapped spin system through the demonstration of triplon SSE in CuGeO_3 . Subsequently, Xing *et al.*²³⁶ reported the SSE in a spin-gapped quantum magnet $\text{Pb}_2\text{V}_3\text{O}_9$ and found a peak behavior at around the critical field B_c for the Bose–Einstein condensation states of triplons. These works show that SSE can be a probe for spin excitations in gapped spin systems, and therefore be applied to other materials with exotic spin ex-

citations, such as spin ladder systems and Shastry–Sutherland systems.

4. Nuclear-spin Seebeck effect

Until recently, all the SSEs have been an exclusive feature of electron spins or orbitals, so they inevitably disappear at ultralow temperatures or high fields due to the entropy quenching^{150,156}. In a solid, there is a hitherto unexplored spin and entropy carrier that is well activated even at such an environment: a nuclear spin. Because of its tiny gyromagnetic ratio γ_n ($\sim 10^3$ times less than that of electrons γ), a nuclear spin exhibits much lower excitation energy than that of electron spins in ambient fields²³⁷, allowing its thermal agitation. In 2021, Kikkawa *et al.*²³⁸ reported an observation of the nuclear-spin Seebeck effect. The material of choice is MnCO_3 , having a large nuclear spin ($I = 5/2$) of ^{55}Mn nuclei and strong hyperfine coupling²³⁹, with Pt contact. The observed nuclear SSE is enhanced down to 100 mK and is not suppressed even under the strong field 14 T, distinct from the electronic SSEs [Fig. 9(c)]. The voltage features are attributed to entropic nuclear-spin excitation with the tiny energy scale of $\sim 30 \text{ mK}$, which is little affected by the field. The result is quantitatively reproduced by a nuclear SSE theory in which interfacial Korringa process²⁴⁰ is taken into consideration²³⁸ [see Figs. 9(a) and 9(c)]. The work may serve as the bridge between nuclear-spin science and thermoelectricity. The spin-current mechanism based on the Korringa relaxation may be important to find other nuclear spintronic phenomena.

C. Spin Peltier effect

Onsager’s reciprocity relation indicates the existence of the Onsager equivalent of SSE: spin Peltier effect (SPE) referring to the heat-current generation as a result of a spin current in

a metal/magnet system²⁴¹. In the SPE, a charge current, \mathbf{J}_c , applied to a metal induces a spin accumulation at the interface with the magnet due to the SHE^{147,148}, which creates or annihilates a magnon in the magnet via the interfacial spin-exchange interaction [see Fig. 7(b)]. Because of the energy conservation, this process accompanies a heat (energy) transfer between the electron in the metal and the magnon in the magnet, leading to a temperature difference between these systems. Experimentally, the SPE-induced temperature modulation has been detected with a thermocouple^{131,241,242}, lock-in thermography (LIT)^{243–248}, lock-in thermoreflectance²⁴⁹, and a heat-flux sensor based on Peltier cells²⁵⁰. The reciprocal relation between the SPE and SSE is addressed both experimentally and theoretically in Refs. 248, 250–252.

So far, a few papers address the SPE at low temperatures^{131,247}. By means of LIT, Yagmur *et al.*²⁴⁷ measured the T dependence of the SPE in a Pt/Gd₃Fe₅O₁₂ system from 300 to 281 K and observed a sign change at around the magnetic compensation temperature $T_{\text{comp}} = 288$ K for Gd₃Fe₅O₁₂. The SPE in this system is expected to show another sign change at a further low T of ~ 71 K due to the competition of multiple magnon modes, but it is not accessible easily through the LIT method as the output infrared emission intensity ($\propto T^4$) is very weak at such a temperature range²⁴⁷. Yahiro *et al.*¹³¹ investigated the magnon-polaron SPE in a Pt/Lu₂Bi₁Fe₄Ga₁O₁₂ system down to 100 K using a thermocouple sensor, but found the difficulty for further low- T measurements as the thermocouple becomes less sensitive with decreasing T . Different types of thermometry would thus be required to further investigate the SPEs at low temperatures and for a wide range of materials.

V. SPIN-MECHANICAL COUPLING

Spin mechanical coupling played a crucial role in developing the quantum mechanics. The coupling between the spin of an electron and mechanical rotation provided the first experimental proof that an electron has an angular momentum i.e., spin, which was reported by Einstein and de-Haas, and Barnett in 1915^{17,18,253,254}. Nowadays, these effects are known as the Einstein-de-Haas (EdH) effect and the Barnett effect. The EdH effect is the phenomenon, in which when a magnetic material is magnetized by applying a magnetic field, such that the spin angular momentum is aligned, the material is mechanically rotated due to the angular momentum conservation law as shown in Fig. 10(a)^{17,254}. The reverse of the EdH effect is referred to as the Barnett effect, in which a mechanically rotating magnet is magnetized as shown in Fig. 10(b)^{18,253}. By using these results, they experimentally determined the value of the g factor of an electron to be ~ 2 prior to the establishment of the modern quantum physics. The EdH has been exploited to determine the g factors of electrons and the orbital component of the magnetic moment in various materials^{255,256}.

The classical analog of the Barnett effect is the Coriolis force acting on the angular momentum in a rotating frame of reference²⁵⁷. As shown in Fig. 11(a), when a rotating matter such as a spinning gyrotrop, which has an angular momentum,

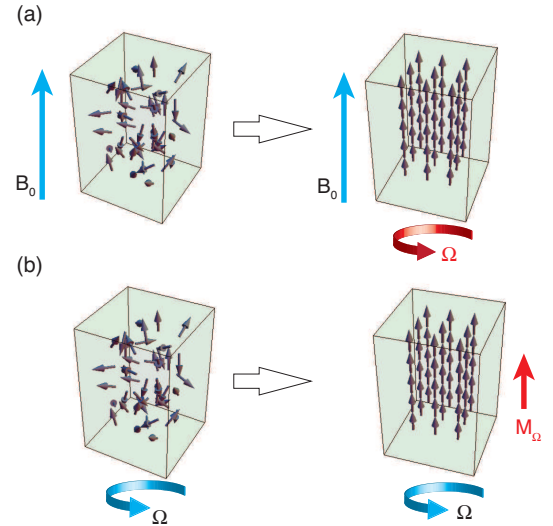


FIG. 10. Schematic illustrations of (a) the Einstein-de-Haas effect and (b) the Barnett effect.

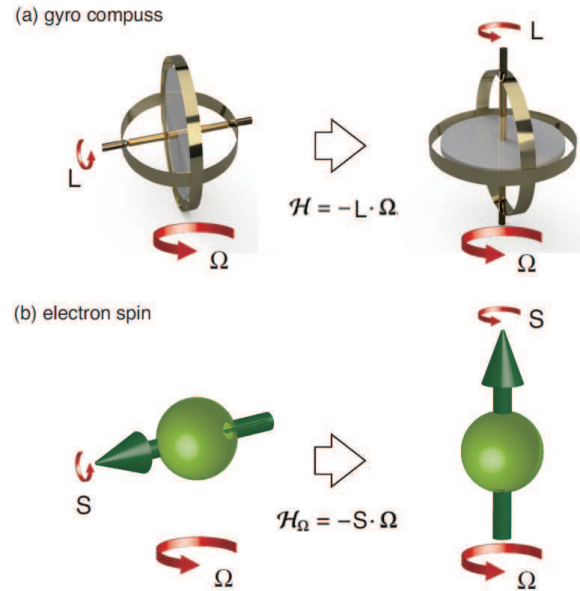


FIG. 11. Schematic illustrations of (a) a gyro compass and (b) spin-rotation coupling.

is externally rotated, namely in the rotating frame of reference, the rotation axis of the gyrotrop aligns in parallel to the external rotation axis. The Hamiltonian of this phenomenon is expressed as

$$\mathcal{H} = -\mathbf{L} \cdot \boldsymbol{\Omega} \quad (27)$$

where \mathbf{L} is the angular momentum of the spinning gyrotrop and $\boldsymbol{\Omega}$ is the angular velocity of the external rotation. The application of this phenomena is a gyro compass, which has navigated vessels since it was invented in 1885. In the case

of a gyro compass, the external rotation is the rotation of the earth, and the rotation axis of the gyro compass points along the rotation axis of the earth.

From the perspective of quantum dynamics, quantum spin angular momentum \mathbf{S} also couples to external rotation. The Hamiltonian is expressed as

$$\mathcal{H}_\Omega = -\mathbf{S} \cdot \boldsymbol{\Omega} \quad (28)$$

This coupling is referred to as the spin-rotation coupling, and is rigorously derived from the general relativistic quantum theory^{258,259}. The spins in the rotating material align in parallel to the direction of the rotation axis, and so do the magnetic moments accompanied with the spins. As a result, the rotating material is magnetized. This is the mechanism of the Barnett effect. As shown in Eq. (28), the external rotation couples with the spin angular momentum similarly to how the magnetic field \mathbf{B} couples with the magnetic moment, which is referred to as the Zeeman interaction $\mathcal{H}_Z = -\mathbf{M} \cdot \mathbf{B}$. As the Zeeman interaction is the most fundamental coupling for measuring the magnetization, we might be able to say that the Barnett effect is the most fundamental phenomenon for measuring the spin angular momentum in the material.

Along with latest advances in physics and technology, the coupling between a spin and mechanics has once again attracted attention especially in terms of spintronics. The EdH effect has been exploited to mechanically manipulate micro devices using a spin angular momentum such as cantilever and paddles^{260,261}. The Barnett effect has been also exploited to generate a spin current from mechanical motion such as fluid flows and surface acoustic waves²⁶²⁻²⁶⁴.

A. Barnett effects

The Barnett effect had been studied only in ferromagnets with large magnetization only at room temperature before our studies have been started. However, considering that the origin of the Barnett effect is the spin-rotational coupling acting on a spin of a single particle, the Barnett effect should be observed for not only paramagnetic materials but also nuclear spin systems. In this section, we first show the experimental results of the observation of the Barnett field B_Ω acting on nuclei by using the NMR and the nuclear quadrupole resonance (NQR) methods²⁶⁵⁻²⁶⁸.

1. Barnett field observed by NMR and NQR

The B_Ω is the inertial magnetic field acting on the particle possessing finite gyromagnetic ratio γ in the rotating frame of reference. The B_Ω can be derived from Eq. (28) as follows,

$$\mathcal{H}_\Omega = -\mathbf{S} \cdot \boldsymbol{\Omega} = -\gamma \mathbf{S} \cdot \mathbf{B}_\Omega \quad (29)$$

where S and Ω are the magnitude of \mathbf{S} and $\boldsymbol{\Omega}$, respectively, and $B_\Omega = \Omega/\gamma$.

Here, in the field of magnetic resonance methods such as ESR and NMR, Ω/γ is the same form as the so-called fictitious or ghost field ω_L/γ , which emerges in the rotating

frame of reference with the Larmor frequency ω_L . In standard textbooks of magnetic resonance methods, to simplify the spin dynamics excited by the rf field or microwave under a static external magnetic field, classical Newtonian rotational coordinate transformation with the angular velocity of ω_L is introduced^{269,270}. Due to these misleading names such as 'fictitious' or 'ghost' fields, it has been often misinterpreted that these fields as a non-real field, which here means that these fields do not lift the energy level of spin states splitted by the Zeeman interaction due to the external field and do not generate magnetization^{271,272}. Nevertheless, the fictitious or ghost field described as ω_L/γ can cancel the existent external magnetic field out in the rotational frame of reference. Therefore, the interpretation of the fictitious or ghost field has been ambiguous as long as considering in the framework of the Newtonian mechanics. On the basis of the general gauge theory, however, ω_L/γ emerging in the rotational frame of reference is the inertial electromagnetic field caused by the rotational coordinate transformation. Furthermore, the inertial field cannot be locally distinguishable from a real field^{258,259,273,274}. This fact is guaranteed by the equivalence principle. Then, we would like to mention our interpretation on why ω_L/γ is called the fictitious or ghost field. The reason is very simple, i.e., a sample is stationary in the usual magnetic resonance. Although a sample is stationary, virtually the rotational coordinate transformation is introduced and considered ω_L/γ so as to simplify the spin dynamics. Therefore, in reality, ω_L/γ does not act on the stationary sample. Thus, generally ω_L/γ induced by the rotational coordinate transformation is called fictitious or ghost field. However, when the sample is actually rotating, Ω/γ acts as a real field on a spin of particle possessing a finite γ value in the rotating sample. With this view point, the Barnett effect, in which mechanical rotation induces magnetization, can be simply described to be $M_\Omega = \chi B_\Omega$, where M_Ω is a magnetization induced by the mechanical rotation and χ is a magnetic susceptibility of the sample²⁷³⁻²⁷⁶. Hereafter, first we demonstrate the observation of the Barnett field B_Ω in the rotating sample by NMR and NQR methods.

To observe the Barnett field, the signal detector, which is a pickup coil in the case of NMR and NQR, must be in the same rotating frame of reference as the rotating sample because the Barnett field is an inertial field emerges on the rotating frame of reference. To overcome this difficulty, we have developed a new NMR (NQR) tuning circuit with a capability for high speed rotation as shown in Fig. 12(a). The rf field generated at the NMR spectrometer is transmitted into the inner tuning circuit through the mutual induction between the stationary coil and the coupling coil. These two coils are electromagnetically coupled, but mechanically decoupled. Thus, we can keep electromagnetic coupling during the high speed rotation of the inner circuit. The key technology of this setup is wireless connection between a rotating frame and a laboratory frame, which enables us to observe the spin dynamics on the rotating frame of reference. In Fig. 12(b), we show the tuning circuit and the high speed rotor used in the study described here²⁶⁵. The tuning circuit is embedded into the epoxy resin to prevent centrifugal damage due to the high speed rotation. The sample is put into the sample coil, and both the

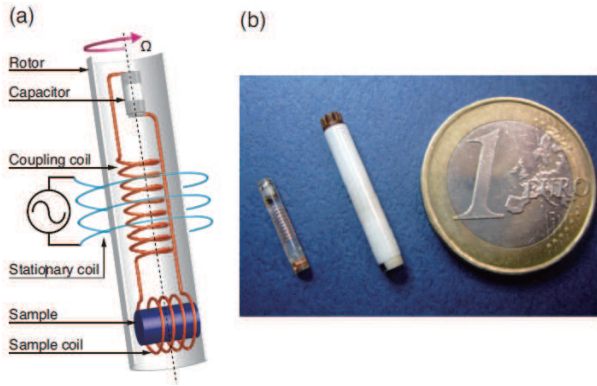


FIG. 12. (a) Illustration of the NMR (NQR) tuning circuit capable of high speed rotation. (b) NMR (NQR) tuning circuit and the high speed rotor.

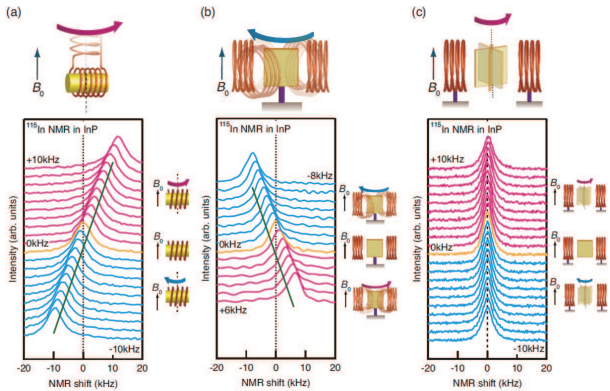


FIG. 13. ^{115}In NMR spectra in InP obtained by using the setup with (a) simultaneous sample coil and sample rotation, (b) only the sample coil rotation, and (c) only the sample rotation.

sample and the circuit are put into this high speed rotor. Then, we blow compressed air to the air turbine to rotate the rotor. In addition, this technique enables us to rotate only the sample coil with the sample fixed in the stationary laboratory frame of reference. Using these techniques, we systematically study the effects of rotation in the setups involving only the sample coil rotation, only the sample rotation, and simultaneous both the sample coil and sample rotation. Applying these setups to NMR and NQR measurements, we observe the NMR line shifts and NQR line splittings, in which the spectral structures are clearly distinct depending on the setups.

Figure 13(a) shows the ^{115}In NMR in InP using the setup shown in Fig. 12(a) under the external magnetic field parallel to the rotation axis. With positive rotation, the NMR shift proportionally increases by increasing the rotation frequency. By contrast, with negative rotation, the NMR shift proportionally decreases by decreasing the rotation frequency. The value of the NMR shift Δf coincides with the rotation frequency $\Omega/2\pi$, i.e., $2\pi\Delta f = \gamma B_\Omega = \Omega$. This behavior is completely consistent with the Barnett field B_Ω acting on the nuclei in the rotating sample.

Using the setup in Fig. 12(a), we have been able to conduct NMR measurement in the rotating frame. Then, we customized this setup to rotate only the sample coil with the sample fixed in the laboratory frame of reference. In this way, we can observe the effect of the relative rotational motion between the sample coil and sample using NMR. The results are shown in Fig. 13(b). The NMR shift also occurs by the relative rotational motion. The value of the NMR shifts coincides with the rotation frequency $\Omega/2\pi$. Thus, we call this NMR shift the rotational Doppler effect. It should be noted here that, even though the value of the NMR shifts arising from the Barnett effect and the rotational Doppler effect is equivalent, their origins are different between them. In the former case, there is no relative rotation between the sample coil and sample, therefore, NMR shift arises from the inertial magnetic field so-called the Barnett field. The latter arises from the relative rotational motion between the sample coil and sample because the sample is in the laboratory frame of reference. Figure 13(c) show the NMR spectra with the setup of only the sample rotation. In this case, there is no NMR shift. The reason for this is that both the Barnett field and rotational Doppler effect are existent. In the case of sample rotation, the direction of the relative rotation is opposite to the rotational direction of the sample. Therefore these effects cancel each other out, so that there is no NMR shift because the absolute values of the NMR shifts in both effects are equivalent.

However, there is a criticism that the both NMR shift shown in Figs. 13(a) and (b) is the same origin, i.e., sample rotation is irrelevant and, thus, coil rotation causes the NMR shift and the Barnett field is unnecessary hypothesis²⁷². In this interpretation, it can be only thought that nuclear spins inside a rotating sample isolate from the rotational motion of the sample. However, as we claim in section V, the nuclear spin in the rotating sample is in the rotating frame of reference and, thus, the spin rotation coupling acts on the nuclear spin. Thus, the Barnett field as the inertial magnetic field in the rotation frame of reference acts on the nuclear spins. Therefore, the interpretation that nuclear spins in a rotating sample isolate from the rotating sample is irrelevant. In the next paragraph, we provide the experimental explicit evidence that nuclear spin in the rotating sample couple with the rotational motion of the sample²⁶⁸.

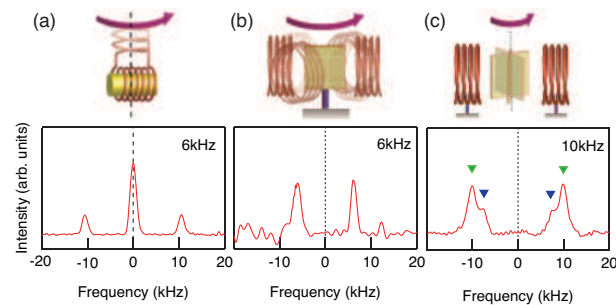


FIG. 14. ^{35}Cl NQR spectra in NaClO_3 obtained by using the setup of (a) simultaneous sample coil and sample rotation, (b) only sample coil rotation, and (c) only sample rotation.

Figure 14 shows ^{35}Cl NQR spectra in the single crystal of NaClO_3 obtained by the setup of (a) the simultaneous sample and sample coil rotation, (b) only the sample coil rotation, (c) only the sample rotation. The rotation axes are parallel to the $\langle 100 \rangle$ direction of the single crystal. In the case of the simultaneous sample and sample coil rotation, the NQR spectra split into three lines with the NQR shifts of $\pm\sqrt{3}\Omega/2\pi$. This spectral structure can be reproduced by treating the Barnett field as a perturbation to the primal quadrupole Hamiltonian. This result is the explicit proof of the existence of the Barnett field in the rotating frame of reference. By contrast, in the case of only the sample coil rotation, the NQR spectra split into two lines with the NQR shifts of $\pm\Omega/2\pi$. This NQR line splitting is caused by the relative rotational motion between the sample and sample coil, namely, the rotational Doppler effect. Compared with these two NQR spectra, it is obvious that the simultaneous sample and sample coil rotation observes definitely different phenomena from the only the sample coil rotation. In the case of just sample rotation shown in Fig. 14(c), a different NQR spectral structure is also observed compared to Fig. 14(a) and (b), meaning that the NQR shift due to the Barnett field and the rotational Doppler effect do not cancel each other out. This result is critically different from the NMR results as shown in Fig. 13(c). For more details about the analysis of the NQR spectra, please refer to the Ref. 268.

2. Barnett effect on paramagnet

We demonstrate the experimental results of the Barnett effect in electronic spin systems of paramagnetic state²⁷⁷. To observe the Barnett effect on the paramagnetic state, we first targeted Gd as a sample because Gd has a large magnetic moment arising from the seven 4f electrons. In addition, Gd shows ferromagnetic transition near room temperature (292 K). Therefore, at just above 292 K, Gd has a large magnetization even in the paramagnetic state. By improving the accuracy of apparatus, e.g. stabilizing the temperature and strengthening the magnetic shield, we succeeded to observe the Barnett effect also on Tb and Dy^{277,278}. 4f electrons are positioned in the inner core inside ions, and have a local magnetic moment isolated from the lattice system. This situation is similar to the nuclear spin system. Therefore, as the Barnett effect of the 4f electron system can be observed, the 4f electron in the rotating frame of reference feels the Barnett field as an inertial magnetic field in the rotating frame of reference.

Figure 15 shows the experimental setup for observing the Barnett effect. The cylindrically shaped sample is inserted into the high speed rotor. The rotor is installed into the high-speed rotation system, which consists of an air bearing and two driving air channels. The rotation system is originally produced by JEOL for magic angle spinning NMR measurements and is improved to realize the two way rotation, that is, backward and forward direction. High speed rotation is realized by blowing compressed air to the air turbine attached at the sample tube. By switching the direction of the air flow, the rotational direction can be reversed. The fluxgate mag-

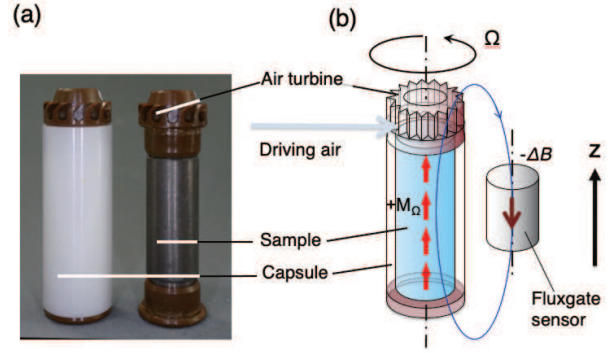


FIG. 15. Experimental setup for observation of the Barnett effect. (a) High speed rotor (left) and sample (right). (b) Illustration of the setup. The directions of magnetization, stray field detected by fluxgate sensor, and rotation are defined as indicated by arrows.

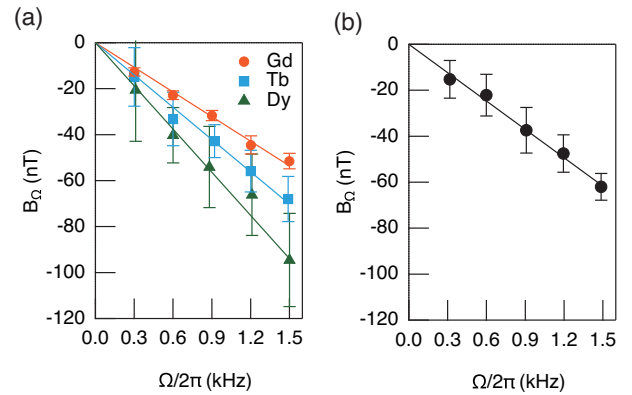


FIG. 16. The Barnett field of (a) Gd, Tb, and Dy, and (b) FeCo nanogranule, respectively.

netic sensor mounted adjacent to the rotation system measures the stray field ΔB from the sample magnetized by the Barnett effect. The definition of the directions of magnetization, the stray field, and rotation are shown in Fig. 15(b). The rotation system and the fluxgate magnetic sensor are enclosed in the magnetic shield made of permalloy. The magnetic shield is composed of two layers. To stabilize the temperature, the whole apparatus is placed inside a thermal isolation chamber, where the temperature is controlled within ± 0.1 K using a high precision air controller. All the measurements were performed at room temperature. The magnetization by the Barnett effect M_Ω is estimated from ΔB by using the dipole model. The Barnett field B_Ω is estimated from M_Ω/χ .

Figure 16(a) shows the rotation frequency dependence of the Barnett field. The negative slopes of the data indicate the antiparallel coupling between the spin and the magnetic moment due to the negative charge of an electron. The gyroscopic g' factor can be estimated from the Barnett field using the equation of $B_\Omega = \frac{2m_e}{g'e}\Omega$, where m_e is the mass of electron, e is the elemental charge of electron and g' is the gyroscopic g factor. The g' factors are estimated to be

2.00 ± 0.08 , 1.53 ± 0.17 , and 1.15 ± 0.32 for Gd, Tb, and Dy, respectively²⁷⁸. These values are very close to the Lande's g factor which is 2, 3/2, and 4/3 for Gd, Tb, and Dy, respectively. This fact indicates that the 4f electron states are well described by the LS coupling scheme.

In the case of 3d electron systems, the magnetic moment mainly arises from the spin component. The gyroscopic g' factor can be used to estimate the orbital contribution to the magnetic moment. To demonstrate this, we measure the Barnett effect on the super paramagnet, which has the large magnetization comparable to the ferromagnet and behaves paramagnetically²⁷⁹. The sample is the FeCo nanogranules embedded in a matrix of MgF₂²⁸⁰. Figure 16(b) shows the rotation speed dependence of the Barnett field. Form the slope of the data, the gyroscopic g' factor is estimated to be 1.76 ± 0.11 ²⁷⁹. When the magnetic moment completely arises from the spin component, g' becomes 2 as is the case with Gd, which has no orbital moment. However, when the orbital component contributes to the magnetic moment, g' becomes smaller than 2. While the g' factor of the bulk FeCo is 1.916, the g' factor of FeCo nanogranules is smaller than the bulk one²⁸¹. This result indicates that the orbital contribution to the magnetic moment in FeCo nanogranules is larger than the bulk one because orbital magnetism is enhanced due to the symmetry breaking of the electron system at the surface of the nanogranules and the fraction of the surface of FeCo nanogranules is larger than the bulk one²⁸².

B. Angular momentum compensation observed by the Barnett effect

Hereafter, we introduce the new application of the Barnett effect. The Barnett effect can measure an angular momentum in a material. Therefore, we challenged to measure the angular momentum compensation temperature in ferrimagnets using the Barnett effect^{283,284}. The angular momentum compensation is the singularity, where the net angular momentum in the material vanishes at a certain temperature. The angular momentum compensation typically exists in the N-type ferrimagnet, which has the magnetic compensation temperature T_M ²⁸⁵. Ferrimagnets consist of two (or more) sublattice possessing different values of the magnetic moments, which couples in antiparallel each other. When the temperature dependence of the order parameter at two sublattice is different from each other, the magnetization at the two sublattice becomes equivalent at a certain temperature, which is T_M . In a general case, when g factors of the magnetic moment at each sublattice are different from each other, the temperature at which the angular momentum at each sublattice becomes equivalent may be different from T_M . This temperature is the angular momentum compensation temperature T_A . To measure T_A by the Barnett effect, we developed the temperature controllable equipment ranging from room temperature down to 120 K as shown in Fig. 17(a)²⁸³. The rotation system is installed in the cryostat and cooled by the nitrogen gas evaporated from liquid nitrogen. The bearing and driving gas were high pressed nitrogen instead of the compressed air and cooled at the heat

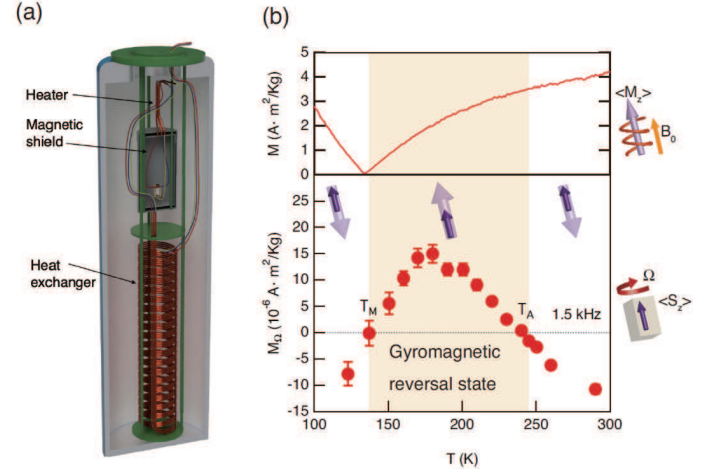


FIG. 17. (a) Schematic of the temperature controllable equipment for observation of the Barnett effect at low temperatures. (b) Temperature dependence of the magnetization induced by the magnetic field (upper panel) and the M_Q induced by the Barnett effect (lower panel) in $\text{Ho}_3\text{Fe}_5\text{O}_{12}$ (HoIG). Light and dark purple arrows represent the net magnetic moment and net angular momentum, respectively.

exchanger inside the cryostat. Then, the temperature of the cooled high pressed nitrogen gas is controlled by the heater. The rotation system is inside the magnetic shield.

Figure 17(b) shows the temperature dependence of the magnetization induced by the magnetic field (upper panel) and the M_Q induced by the Barnett effect (lower panel) in $\text{Ho}_3\text{Fe}_5\text{O}_{12}$ (HoIG). In the upper panel, the magnetization disappears at 135 K. This temperature is the magnetic compensation temperature T_M . In the lower panel, the M_Q also disappears at 135 K. This is a trivial behavior because even though the spin responds to the rotation and aligns to the rotation axis due to the Barnett effect, the magnetization is basically zero. Thus the M_Q also becomes zero. Interestingly, the M_Q also disappears at 240 K despite the finite spontaneous magnetization at 240 K as shown in the upper panel in Fig. 17(b). This temperature is T_A . Although, at T_A , the spontaneous magnetization has a finite value, the net angular momentum is compensated and, thus, the Barnett effect does not occur. The T_A is also observed by the NMR measurement in HoIG, in which the NMR intensity is enhanced at T_A ^{286,287}. At the temperatures between 135 K and 240 K, the M_Q takes positive values, while, above 240 K and below 135 K, takes negative values. As shown in Figs. 16(a) and 16(b) the $M_Q = \chi B_\Omega$ usually shows negative values due to the antiparallel coupling between a spin and a magnetic moment. Thus, the positive values of the M_Q indicate the parallel coupling between a spin and a magnetic moment. We call this reversal of the coupling the gyromagnetic reversal state.

The angular momentum compensation is thought to be a promising candidate to quicken the speed of magnetization switching, which is important for speeding up the magnetic device using the direction of magnetization as an information carrier because, at T_A , there is no inertia due to the vanishment

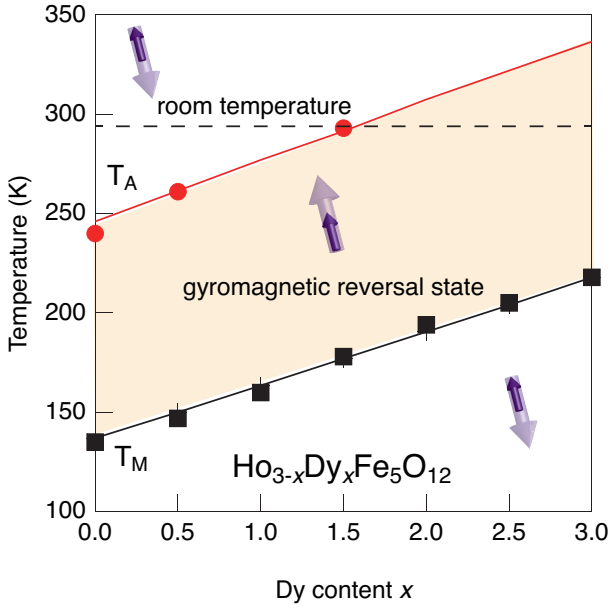


FIG. 18. Gyromagnetic phase diagram of $\text{Ho}_{3-x}\text{Dy}_x\text{Fe}_5\text{O}_{12}$. Black square and red circle represent T_M and T_A , respectively. The beige area represents the gyromagnetic reversal state. Light and dark purple arrows represent the net magnetic moment and net angular momentum, respectively.

of a net angular momentum in materials. Thus, manipulation of the angular compensation temperature to room temperature is an important subject for future high-speed magnetic devices. Recently, we demonstrated the manipulation of T_A in HoIG as a platform by partially substituting Dy for Ho. The T_A is determined by the Barnett effect. The results are shown in Fig. 18^{284,286}. Both T_M and T_A increase with the increase of the Dy content. The T_A value coincides with room temperature (293 K) at the composition of $\text{Ho}_{1.5}\text{Dy}_{1.5}\text{Fe}_5\text{O}_{12}$. Using the Barnett effect, we can conveniently determine the T_A values in any samples irrespective of electronic conductivity of the sample and the sample state; single crystals, powders, poly-crystals, and thin films are all available. Thus, our studies pave the new way to explore new materials possessing T_A , which will be utilized for magnetic devices in the future.

VI. CONCLUSIONS

In this article, we gave an overview on current studies of spin, spin current, and their related phenomena based on the authors' expertise. The topics include spin pumping, spin Seebeck and Peltier effects, spin transfer and topological Hall torques, emergent inductor, and also spin-mechanical/lattice coupling phenomena, where both the electron and nuclear spins and their angular-momentum conversion play an important role.

Nowadays, the concept of spin current has emerged in various areas of condensed matter physics and has played a role as a useful guiding principle to open up new phenomena in con-

densed matter. Moreover, the concept of spin current appears not only in physics but also in various fields of science and technology. The diversity of materials and device structures has expanded the possibilities of application of spin currents, and such cross-disciplinary expansion is an important aspect of this field. Another interesting physical aspects of spin currents are their universality, which explains a wide range of phenomena in a unified manner with a small number of principles, and their power to predict unknown physical phenomena based on this universality. We anticipate that spin current and its versatile coupling with other physical entities may play an essential role in future electronic devices and technologies including quantum information science and energy harvesting.

ACKNOWLEDGMENTS

The authors thank T. Makiuchi, T. Hioki, H. Ariawa, Y. Yamane, Y. Araki, M. Matsuo, M. Imai, K. Harii, Y. Ogata, M. Sato, and Y. Ohnuma for valuable discussions, Y. Haga for the X-ray diffraction experiment and M. Ono for technical supports. This work was financially supported by JST ERATO "Spin Quantum Rectification Project" (Grant No. JP- MJER1402), JST CREST (Grants Nos. JPMJCR19J4, JPMJCR1874, JP-MJCR20C1 and JPMJCR20T2), JSPS KAKENHI (Grants Nos. JP19H05600, JP19H05622, JP17H02927, JP20H01863, JP20H01865, JP20H02599, JP21H01800, JP21H04643, and JP22K18686), Grant-in-Aid for Transformative Research Areas (No. JP22H05114), Institute for AI and Beyond of the University of Tokyo, IBM-UTokyo lab, and Daikin Industries, Ltd.

AUTHOR DECLARATIONS

Conflict of Interest

The authors have no conflicts to disclose.

Author Contributions

Sadamichi Maekawa: Conceptualization (equal); Writing – original draft (equal); Writing – review & editing (equal). **Takashi Kikkawa:** Conceptualization (equal); Writing – original draft (equal); Writing – review & editing (equal). **Hiroyuki Chudo:** Writing – original draft (equal); Writing – review & editing (equal). **Jun'ichi Ieda:** Conceptualization (equal); Writing – original draft (equal); Writing – review & editing (equal). **Eiji Saitoh:** Conceptualization (equal); Writing – original draft (equal); Writing – review & editing (equal).

DATA AVAILABILITY

The data that support the findings of this study are available from the corresponding author upon reasonable request.

¹S. Maekawa, E. Saitoh, S. O. Valenzuela, and T. Kimura, eds., *Spin Current*, 2nd ed. (Oxford University Press, Oxford, 2017).

²S. Maekawa, H. Adachi, K.-i. Uchida, J. Ieda, and E. Saitoh, *J. Phys. Soc. Jpn.* **82**, 102002 (2013).

³J. E. Hirsch, *Phys. Rev. Lett.* **83**, 1834 (1999).

⁴E. Saitoh, M. Ueda, H. Miyajima, and G. Tatara, *Appl. Phys. Lett.* **88**, 182509 (2006).

⁵A. Azevedo, L. H. Vilela Leão, R. L. Rodríguez-Suárez, A. B. Oliveira, and S. M. Rezende, *J. Appl. Phys.* **97**, 10C715 (2005).

⁶S. O. Valenzuela and M. Tinkham, *Nature* **442**, 176 (2006).

⁷M. V. Costache, M. Sladkov, S. M. Watts, C. H. van der Wal, and B. J. van Wees, *Phys. Rev. Lett.* **97**, 216603 (2006).

⁸T. Kimura, Y. Otani, T. Sato, S. Takahashi, and S. Maekawa, *Phys. Rev. Lett.* **98**, 156601 (2007).

⁹J. C. Slonczewski, *Phys. Rev. B* **39**, 6995 (1989).

¹⁰J. Slonczewski, *J. Magn. Magn. Mater.* **159**, L1 (1996).

¹¹L. Berger, *Phys. Rev. B* **54**, 9353 (1996).

¹²E. B. Myers, D. C. Ralph, J. A. Katine, R. N. Louie, and R. A. Buhrman, *Science* **285**, 867 (1999).

¹³A. Stern, *Phys. Rev. Lett.* **68**, 1022 (1992).

¹⁴N. Nagaosa and Y. Tokura, *Physica Scripta* **T146**, 014020 (2012).

¹⁵N. Nagaosa and Y. Tokura, *Nat. Nanotechnol.* **8**, 899 (2013).

¹⁶S. E. Barnes and S. Maekawa, *Phys. Rev. Lett.* **98**, 246601 (2007).

¹⁷A. Einstein and W. J. de Haas, *Deutsche Physikalische Gesellschaft*, **17**, 152 (1915).

¹⁸S. J. Barnett, *Phys. Rev.* **6**, 239 (1915).

¹⁹M. I. D'yakonov and V. I. Perel', *Zh. Eksp. Teor. Fiz.* **T146**, 014020 (1971).

²⁰R. J. Elliott, *Phys. Rev.* **96**, 266 (1954).

²¹Y. Yafet, *Solid State Physics*, **14**, 1 (1963).

²²Y. Kajiwara, K. Harii, S. Takahashi, J. Ohe, K. Uchida, M. Mizuguchi, H. Umezawa, H. Kawai, K. Ando, K. Takanashi, S. Maekawa, and E. Saitoh, *Nature* **464**, 262 (2010).

²³A. Hirohata, K. Yamada, Y. Nakatani, I.-L. Prejbeanu, B. Diény, P. Pirro, and B. Hillebrands, *J. Magn. Magn. Mater.* **509**, 166711 (2020).

²⁴B. Dieny, I. L. Prejbeanu, K. Garello, P. Gambardella, P. P. Freitas, R. Lehndorff, W. Raberg, U. Ebels, S. O. Demokritov, J. Akerman, A. Deac, P. Pirro, C. Adelmann, A. Anane, A. V. Chumak, A. Hirooata, S. Mangin, M. C. Onbasli, M. d. Aquino, G. Prenat, G. Finocchio, L. L. Diaz, R. Chantrell, O. C. Fesenko, and P. Bortolotti, *Nat. Electron.* **3**, 446 (2020).

²⁵S. Mizukami, Y. Ando, and T. Miyazaki, *Phys. Rev. B* **66**, 104413 (2002).

²⁶Y. Tserkovnyak, A. Brataas, and G. E. W. Bauer, *Phys. Rev. Lett.* **88**, 117601 (2002).

²⁷K. Ando, S. Takahashi, J. Ieda, Y. Kajiwara, H. Nakayama, T. Yoshino, K. Harii, Y. Fujikawa, M. Matsuo, S. Maekawa, and E. Saitoh, *J. Appl. Phys.* **109**, 103913 (2011).

²⁸L. Berger, *Phys. Rev. B* **33**, 1572 (1986).

²⁹G. E. Volovik, *J. Phys. C: Solid State Physics* **20**, L83 (1987).

³⁰S. A. Yang, G. S. D. Beach, C. Knutson, D. Xiao, Q. Niu, M. Tsoi, and J. L. Erskine, *Phys. Rev. Lett.* **102**, 067201 (2009).

³¹P. N. Hai, S. Ohya, M. Tanaka, S. E. Barnes, and S. Maekawa, *Nature* **458**, 489 (2009).

³²Y. Yamane, K. Sasage, T. An, K. Harii, J. Ohe, J. Ieda, S. E. Barnes, E. Saitoh, and S. Maekawa, *Phys. Rev. Lett.* **107**, 236602 (2011).

³³M. Hayashi, J. Ieda, Y. Yamane, J.-i. Ohe, Y. K. Takahashi, S. Mitani, and S. Maekawa, *Phys. Rev. Lett.* **108**, 147202 (2012).

³⁴J. Ieda, Y. Yamane, and S. Maekawa, *SPIN* **03**, 1330004 (2013).

³⁵K. M. D. Hals and A. Brataas, *Phys. Rev. B* **91**, 214401 (2015).

³⁶Y. Yamane and J. Ieda, *J. Magn. Magn. Mater.* **491**, 165550 (2019).

³⁷A. Soumyanarayanan, N. Reyren, A. Fert, and C. Panagopoulos, *Nature* **539**, 509 (2016).

³⁸J. Ye, Y. B. Kim, A. J. Millis, B. I. Shraiman, P. Majumdar, and Z. Tešanović, *Phys. Rev. Lett.* **83**, 3737 (1999).

³⁹G. Tatara and H. Kawamura, *J. Phys. Soc. Jpn.* **71**, 2613 (2002).

⁴⁰M. Lee, W. Kang, Y. Onose, Y. Tokura, and N. P. Ong, *Phys. Rev. Lett.* **102**, 186601 (2009).

⁴¹A. Neubauer, C. Pfleiderer, B. Binz, A. Rosch, R. Ritz, P. G. Niklowitz, and P. Böni, *Phys. Rev. Lett.* **102**, 186602 (2009).

⁴²N. Kanazawa, Y. Onose, T. Arima, D. Okuyama, K. Ohoyama, S. Wakimoto, K. Kakurai, S. Ishiwata, and Y. Tokura, *Phys. Rev. Lett.* **106**, 156603 (2011).

⁴³G. Tatara, *Physica E: Low-dimensional Systems and Nanostructures* **106**, 208 (2019).

⁴⁴S. E. Barnes, J. Ieda, and S. Maekawa, *Appl. Phys. Lett.* **89**, 122507 (2006).

⁴⁵J. Ieda and S. Maekawa, *Appl. Phys. Lett.* **101**, 252413 (2012).

⁴⁶N. Nagaosa, *Jpn. J. Appl. Phys.* **58**, 120909 (2019).

⁴⁷J. Li, C. B. Wilson, R. Cheng, M. Lohmann, M. Kavand, W. Yuan, M. Al-dosary, N. Agladze, P. Wei, M. S. Sherwin, and J. Shi, *Nature* **578**, 70 (2020).

⁴⁸P. Vaidya, S. A. Morley, J. van Tol, Y. Liu, R. Cheng, A. Brataas, D. Lederman, and E. del Barco, *Science* **368**, 160 (2020).

⁴⁹A. V. Chumak, V. I. Vasyuchka, A. A. Serga, and B. Hillebrands, *Nat. Phys.* **11**, 453 (2015).

⁵⁰M. Althammer, *J. Phys. D: Appl. Phys.* **51**, 313001 (2018).

⁵¹A. Brataas, B. van Wees, O. Klein, G. de Loubens, and M. Viret, *Phys. Rep.* **885**, 1 (2020).

⁵²C. W. Sandweg, Y. Kajiwara, A. V. Chumak, A. A. Serga, V. I. Vasyuchka, M. B. Jungfleisch, E. Saitoh, and B. Hillebrands, *Phys. Rev. Lett.* **106**, 216601 (2011).

⁵³C. Hahn, G. de Loubens, M. Viret, O. Klein, V. V. Naletov, and J. B. Youssef, *Phys. Rev. Lett.* **111**, 217204 (2013).

⁵⁴D. Wei, M. Obstbaum, M. Ribow, C. H. Back, and G. Woltersdorf, *Nat. Commun.* **5**, 3768 (2014).

⁵⁵P. Hyde, L. Bai, D. M. J. Kumar, B. W. Southern, C.-M. Hu, S. Y. Huang, B. F. Miao, and C. L. Chien, *Phys. Rev. B* **89**, 180404(R) (2014).

⁵⁶M. Weiler, J. M. Shaw, H. T. Nembach, and T. J. Silva, *Phys. Rev. Lett.* **113**, 157204 (2014).

⁵⁷L. Bai, M. Harder, Y. P. Chen, X. Fan, J. Q. Xiao, and C.-M. Hu, *Phys. Rev. Lett.* **114**, 227201 (2015).

⁵⁸H. Maier-Flaig, M. Harder, R. Gross, H. Huebl, and S. T. B. Goennenwein, *Phys. Rev. B* **94**, 054433 (2016).

⁵⁹L. Bai, M. Harder, P. Hyde, Z. Zhang, C.-M. Hu, Y. Chen, and J. Q. Xiao, *Phys. Rev. B* **118**, 217201 (2017).

⁶⁰H. Hayashi and K. Ando, *Phys. Rev. Lett.* **121**, 237202 (2018).

⁶¹Y. Li, W. Cao, V. P. Amin, Z. Zhang, J. Gibbons, J. Sklenar, J. Pearson, P. M. Haney, M. D. Stiles, W. E. Bailey, V. Novosad, A. Hoffmann, and W. Zhang, *Phys. Rev. Lett.* **124**, 117202 (2020).

⁶²Y. Fan, J. Finley, J. Han, M. E. Holtz, P. Quarterman, P. Zhang, T. S. Safi, J. T. Hou, A. J. Grutter, and L. Liu, *Adv. Mater.* **33**, 2008555 (2021).

⁶³V. Baltz, A. Manchon, M. Tsoi, T. Moriyama, T. Ono, and Y. Tserkovnyak, *Rev. Mod. Phys.* **90**, 015005 (2018).

⁶⁴O. Gomonay, V. Baltz, A. Brataas, and Y. Tserkovnyak, *Nat. Phys.* **14**, 213 (2018).

⁶⁵T. Moriyama, K. Hayashi, K. Yamada, M. Shima, Y. Ohya, Y. Tserkovnyak, and T. Ono, *Phys. Rev. B* **101**, 060402(R) (2020).

⁶⁶S. M. Rezende, A. Azevedo, and R. L. Rodríguez-Suárez, *J. Appl. Phys.* **126**, 151101 (2019).

⁶⁷H. Qiu, L. Zhou, C. Zhang, J. Wu, Y. Tian, S. Cheng, S. Mi, H. Zhao, Q. Zhang, D. Wu, B. Jin, J. Chen, and P. Wu, *Nat. Phys.* **17**, 388 (2021).

⁶⁸I. Boventer, H. T. Simensen, A. Anane, M. Kläui, A. Brataas, and R. Lebrun, *Phys. Rev. Lett.* **126**, 187201 (2021).

⁶⁹H. Wang, Y. Xiao, M. Guo, E. Lee-Wong, G. Q. Yan, R. Cheng, and C. R. Du, *Phys. Rev. Lett.* **127**, 117202 (2021).

⁷⁰T. Makiuchi, T. Hioki, Y. Shimazu, Y. Oikawa, N. Yokoi, S. Daimon, and E. Saitoh, *Appl. Phys. Lett.* **118**, 022402 (2021).

⁷¹T. Hioki, H. Shimizu, T. Makiuchi, and E. Saitoh, *Phys. Rev. B* **104**, L100419 (2021).

⁷²H. Shimizu, T. Hioki, and E. Saitoh, *Appl. Phys. Lett.* **120**, 012402 (2022).

⁷³M. Elyasi, E. Saitoh, and G. E. W. Bauer, "Theory of the magnon parametron," (2021), arXiv: 2109.09117.

⁷⁴A. V. Chumak and *et al.*, *IEEE Trans. Magn.* **58**, 0800172 (2022).

⁷⁵K. Obata and G. Tatara, *Phys. Rev. B* **77**, 214429 (2008).

⁷⁶A. Manchon and S. Zhang, *Phys. Rev. B* **78**, 212405 (2008).

⁷⁷I. Mihai Miron, G. Gaudin, S. Auffret, B. Rodmacq, A. Schuhl, S. Pizzini, J. Vogel, and P. Gambardella, *Nat. Mater.* **9**, 230 (2010).

⁷⁸I. M. Miron, K. Garello, G. Gaudin, P.-J. Zermatten, M. V. Costache, S. Auffret, S. Bandiera, B. Rodmacq, A. Schuhl, and P. Gambardella, *Nature* **476**, 189 (2011).

⁷⁹L. Liu, O. J. Lee, T. J. Gudmundsen, D. C. Ralph, and R. A. Buhrman, *Phys. Rev. Lett.* **109**, 096602 (2012).

⁸⁰L. Liu, C.-F. Pai, Y. Li, H. W. Tseng, D. C. Ralph, and R. A. Buhrman, *Science* **336**, 555 (2012).

⁸¹R. Karplus and J. M. Luttinger, *Phys. Rev.* **95**, 1154 (1954).

⁸²G. Sundaram and Q. Niu, *Phys. Rev. B* **59**, 14915 (1999).

⁸³N. Nagaosa, *J. Phys. Soc. Jpn.* **75**, 042001 (2006).

⁸⁴N. A. Sinitsyn, *J. Phys.: Condens. Matter* **20**, 023201 (2007).

⁸⁵N. Nagaosa, J. Sinova, S. Onoda, A. H. MacDonald, and N. P. Ong, *Rev. Mod. Phys.* **82**, 1539 (2010).

⁸⁶K. Nomura and N. Nagaosa, *Phys. Rev. Lett.* **106**, 166802 (2011).

⁸⁷R. Yu, W. Zhang, H.-J. Zhang, S.-C. Zhang, X. Dai, and Z. Fang, *Science* **329**, 61 (2010).

⁸⁸C.-Z. Chang, J. Zhang, X. Feng, J. Shen, Z. Zhang, M. Guo, K. Li, Y. Ou, P. Wei, L.-L. Wang, Z.-Q. Ji, Y. Feng, S. Ji, X. Chen, J. Jia, X. Dai, Z. Fang, S.-C. Zhang, K. He, Y. Wang, L. Lu, X.-C. Ma, and Q.-K. Xue, *Science* **340**, 167 (2013).

⁸⁹J. G. Checkelsky, J. Ye, Y. Onose, Y. Iwasa, and Y. Tokura, *Nat. Phys.* **8**, 729 (2012).

⁹⁰A. G. Grushin, *Phys. Rev. D* **86**, 045001 (2012).

⁹¹P. Goswami and S. Tewari, *Phys. Rev. B* **88**, 245107 (2013).

⁹²A. A. Burkov, *Phys. Rev. B* **89**, 155104 (2014).

⁹³A. A. Burkov, *Phys. Rev. Lett.* **113**, 187202 (2014).

⁹⁴S. Nakatsuji, N. Kiyohara, and T. Higo, *Nature* **527**, 212 (2015).

⁹⁵N. Kiyohara, T. Tomita, and S. Nakatsuji, *Phys. Rev. Appl.* **5**, 064009 (2016).

⁹⁶A. K. Nayak, J. E. Fischer, Y. Sun, B. Yan, J. Karel, A. C. Komarek, C. Shekhar, N. Kumar, W. Schnelle, J. Kübler, C. Felser, and S. S. P. Parkin, *Sci. Adv.* **2**, e1501870 (2016).

⁹⁷E. Liu, Y. Sun, N. Kumar, L. Muechler, A. Sun, L. Jiao, S.-Y. Yang, D. Liu, A. Liang, Q. Xu, J. Kroder, V. Süß, H. Borrman, C. Shekhar, Z. Wang, C. Xi, W. Wang, W. Schnelle, S. Wirth, Y. Chen, S. T. B. Goennenwein, and C. Felser, *Nat. Phys.* **14**, 1125 (2018).

⁹⁸Q. Wang, Y. Xu, R. Lou, Z. Liu, M. Li, Y. Huang, D. Shen, H. Weng, S. Wang, and H. Lei, *Nat. Commun.* **9**, 3681 (2018).

⁹⁹I. Garate and M. Franz, *Phys. Rev. Lett.* **104**, 146802 (2010).

¹⁰⁰T. Yokoyama, J. Zang, and N. Nagaosa, *Phys. Rev. B* **81**, 241410 (2010).

¹⁰¹D. Pesin and A. H. MacDonald, *Nat. Mater.* **11**, 409 (2012).

¹⁰²Y. Tserkovnyak and D. Loss, *Phys. Rev. Lett.* **108**, 187201 (2012).

¹⁰³A. Sakai and H. Kohno, *Phys. Rev. B* **89**, 165307 (2014).

¹⁰⁴P. B. Ndiaye, C. A. Akosa, M. H. Fischer, A. Vaezi, E.-A. Kim, and A. Manchon, *Phys. Rev. B* **96**, 014408 (2017).

¹⁰⁵D. Kurebayashi and N. Nagaosa, *Phys. Rev. B* **100**, 134407 (2019).

¹⁰⁶Y. Imai, T. Yamaguchi, A. Yamakage, and H. Kohno, *Phys. Rev. B* **103**, 054402 (2021).

¹⁰⁷D. Kurebayashi and K. Nomura, *Phys. Rev. Appl.* **6**, 044013 (2016).

¹⁰⁸D. Kurebayashi, Y. Araki, and K. Nomura, *J. Phys. Soc. Jpn.* **90**, 084702 (2021).

¹⁰⁹D. Kurebayashi and K. Nomura, *Sci. Rep.* **9**, 5365 (2019).

¹¹⁰Y. Araki and J. Ieda, *Phys. Rev. Lett.* **127**, 277205 (2021).

¹¹¹H. Wu, A. Chen, P. Zhang, H. He, J. Nance, C. Guo, J. Sasaki, T. Shirokura, P. N. Hai, B. Fang, S. A. Razavi, K. Wong, Y. Wen, Y. Ma, G. Yu, G. P. Carman, X. Han, X. Zhang, and K. L. Wang, *Nat. Commun.* **12**, 6251 (2021).

¹¹²M. Yamanouchi, Y. Araki, T. Sakai, T. Uemura, H. Ohta, and J. Ieda, *Sci. Adv.* **8**, eab16192 (2022).

¹¹³M. Feigenson, J. W. Reiner, and L. Klein, *Phys. Rev. Lett.* **98**, 247204 (2007).

¹¹⁴M. Yamanouchi, T. Oyamada, K. Sato, H. Ohta, and J. Ieda, *IEEE Trans. Magn.* **55**, 1400604 (2019).

¹¹⁵S. Itoh, Y. Endoh, T. Yokoo, S. Ibuka, J.-G. Park, Y. Kaneko, K. S. Takahashi, Y. Tokura, and N. Nagaosa, *Nat. Commun.* **7**, 11788 (2016).

¹¹⁶T. Yokouchi, F. Kagawa, M. Hirschberger, Y. Otani, N. Nagaosa, and Y. Tokura, *Nature* **586**, 232 (2020).

¹¹⁷J. Ieda and Y. Yamane, *Phys. Rev. B* **103**, L100402 (2021).

¹¹⁸D. Kurebayashi and N. Nagaosa, *Commun. Phys.* **4**, 260 (2021).

¹¹⁹A. Kitaori, N. Kanazawa, T. Yokouchi, F. Kagawa, N. Nagaosa, and Y. Tokura, *Proc. Natl. Acad. Sci. USA* **118**, e2105422118 (2021).

¹²⁰Y. Yamane, S. Fukami, and J. Ieda, *Phys. Rev. Lett.* **128**, 147201 (2022).

¹²¹Y. Aharonov and A. Casher, *Phys. Rev. Lett.* **53**, 319 (1984).

¹²²A. G. Gurevich and G. A. Melkov, *Magnetization Oscillations and Waves* (CRC Press, Boca Raton, FL, 1996).

¹²³F. Keffer, *Spin Waves in Handbuch der Physik*, edited by H. P. J. Wijn, Vol. XVIII/2: Ferromagnetismus (Springer-Verlag, Berlin Heidelberg, 1966).

¹²⁴B. Lüthi, *Physical Acoustics in the Solid State*, 2nd ed. (Springer-Verlag, Berlin Heidelberg, 2007).

¹²⁵H. Arisawa, H. Shim, S. Daimon, T. Kikkawa, Y. Oikawa, S. Takahashi, T. Ono, and E. Saitoh, *Nat. Commun.* **13**, 2440 (2022).

¹²⁶A. Kamra, H. Keshtgar, P. Yan, and G. E. W. Bauer, *Phys. Rev. B* **91**, 104409 (2015).

¹²⁷K. Shen and G. E. W. Bauer, *Phys. Rev. Lett.* **115**, 197201 (2015).

¹²⁸T. Kikkawa, K. Shen, B. Flebus, R. A. Duine, K. Uchida, Z. Qiu, G. E. W. Bauer, and E. Saitoh, *Phys. Rev. Lett.* **117**, 207203 (2016).

¹²⁹B. Flebus, K. Shen, T. Kikkawa, K. Uchida, Z. Qiu, E. Saitoh, R. A. Duine, and G. E. W. Bauer, *Phys. Rev. B* **95**, 144420 (2017).

¹³⁰P. Frey, D. A. Bozhko, V. S. L'vov, B. Hillebrands, and A. A. Serga, *Phys. Rev. B* **104**, 014420 (2021).

¹³¹R. Yahiro, T. Kikkawa, R. Ramos, K. Oyanagi, T. Hioki, S. Daimon, and E. Saitoh, *Phys. Rev. B* **101**, 024407 (2020).

¹³²J. Holanda, D. S. Maior, A. Azevedo, and S. M. Rezende, *Nat. Phys.* **14**, 500 (2018).

¹³³K. An, A. N. Litvinenko, R. Kohno, A. A. Fuad, V. V. Naletov, L. Vila, U. Ebels, G. de Loubens, H. Hurdequin, N. Beaulieu, J. B. Youssef, N. Vukadinovic, G. E. W. Bauer, A. N. Slavin, V. S. Tiberkevich, and O. Klein, *Phys. Rev. B* **101**, 060407(R) (2020).

¹³⁴T. Hioki, Y. Hashimoto, and E. Saitoh, *Commun. Phys.* **3**, 188 (2020).

¹³⁵Y. Li, C. Zhao, W. Zhang, A. Hoffmann, and V. Novosad, *APL Mater.* **9**, 60902 (2021).

¹³⁶B. Z. Rameshti, S. V. Kusminskiy, J. A. Haigh, K. Usami, D. Lachance-Quirion, Y. Nakamura, C.-M. Hu, H. X. Tang, G. E. W. Bauer, and Y. M. Blanter, *Phys. Rep.* **979**, 1 (2022).

¹³⁷K. Uchida, M. Ishida, T. Kikkawa, A. Kirihara, T. Murakami, and E. Saitoh, *J. Phys.: Condens. Matter* **26**, 389601 (2014).

¹³⁸K. Uchida, H. Adachi, T. Kikkawa, A. Kirihara, M. Ishida, S. Yorozu, S. Maekawa, and E. Saitoh, *Proc. IEEE* **104**, 1946 (2016).

¹³⁹T. Kikkawa and E. Saitoh, to appear in Vol. 14 of *Annu. Rev. Condens. Matter Phys.* (2023), (2022), arXiv:2205.10509.

¹⁴⁰J. Xiao, G. E. W. Bauer, K. Uchida, E. Saitoh, and S. Maekawa, *Phys. Rev. B* **81**, 214418 (2010).

¹⁴¹H. Adachi, K. Uchida, E. Saitoh, and S. Maekawa, *Rep. Prog. Phys.* **76**, 036501 (2013).

¹⁴²S. M. Rezende, R. L. Rodríguez-Suárez, R. O. Cunha, A. R. Rodrigues, F. L. A. Machado, G. A. F. Guerra, J. C. L. Ortiz, and A. Azevedo, *Phys. Rev. B* **89**, 014416 (2014).

¹⁴³J. Barker and G. E. Bauer, *Phys. Rev. Lett.* **117**, 217201 (2016).

¹⁴⁴S. M. Rezende, *Fundamentals of Magnonics* (Springer Nature Switzerland AG, Switzerland, 2020).

¹⁴⁵K. Uchida, H. Adachi, T. Ota, H. Nakayama, S. Maekawa, and E. Saitoh, *Appl. Phys. Lett.* **97**, 172505 (2010).

¹⁴⁶Z. Qiu, D. Hou, T. Kikkawa, K. Uchida, and E. Saitoh, *Appl. Phys. Express* **8**, 083001 (2015).

¹⁴⁷A. Hoffmann, *IEEE Trans. Magn.* **49**, 5172 (2013).

¹⁴⁸J. Sinova, S. O. Valenzuela, J. Wunderlich, C. H. Back, and T. Jungwirth, *Rev. Mod. Phys.* **87**, 1213 (2015).

¹⁴⁹K. Uchida, T. Kikkawa, A. Miura, J. Shiomi, and E. Saitoh, *Phys. Rev. X* **4**, 041023 (2014).

¹⁵⁰T. Kikkawa, K. Uchida, S. Daimon, Z. Qiu, Y. Shiomi, and E. Saitoh, *Phys. Rev. B* **92**, 064413 (2015).

¹⁵¹H. Jin, S. R. Boona, Z. Yang, R. C. Myers, and J. P. Heremans, *Phys. Rev. B* **92**, 054436 (2015).

¹⁵²E.-J. Guo, J. Cramer, A. Kehlberger, C. A. Ferguson, D. A. MacLaren, G. Jakob, and M. Kläui, *Phys. Rev. X* **6**, 031012 (2016).

¹⁵³R. Iguchi, K. Uchida, S. Daimon, and E. Saitoh, *Phys. Rev. B* **95**, 174401 (2017).

¹⁵⁴K. Uchida, J. Ohe, T. Kikkawa, S. Daimon, D. Hou, Z. Qiu, and E. Saitoh, Phys. Rev. B **92**, 014415 (2015).

¹⁵⁵L. J. Cornelissen and B. J. van Wees, Phys. Rev. B **93**, 020403(R) (2016).

¹⁵⁶T. Kikkawa, K. Uchida, S. Daimon, and E. Saitoh, J. Phys. Soc. Jpn. **85**, 065003 (2016).

¹⁵⁷A. Miura, T. Kikkawa, R. Iguchi, K. Uchida, E. Saitoh, and J. Shiomi, Phys. Rev. Mater. **1**, 014601 (2017).

¹⁵⁸B. L. Giles, Z. Yang, J. S. Jamison, and R. C. Myers, Phys. Rev. B **92**, 224415 (2015).

¹⁵⁹A. Kehlberger, U. Ritzmann, D. Hinzke, E.-J. Guo, J. Cramer, G. Jakob, M. C. Onbasli, D. H. Kim, C. A. Ross, M. B. Jungfleisch, B. Hillebrands, U. Nowak, and M. Kläui, Phys. Rev. Lett. **115**, 096602 (2015).

¹⁶⁰L. J. Cornelissen, J. Liu, R. A. Duine, J. B. Youssef, and B. J. van Wees, Nat. Phys. **11**, 1022 (2015).

¹⁶¹A. Prakash, B. Flebus, J. Brangham, F. Yang, Y. Tserkovnyak, and J. P. Heremans, Phys. Rev. B **97**, 020408(R) (2018).

¹⁶²H. Wu, L. Huang, C. Fang, B. S. Yang, C. H. Wan, G. Q. Yu, J. F. Feng, H. X. Wei, and X. F. Han, Phys. Rev. Lett. **120**, 097205 (2018).

¹⁶³T. Nozue, T. Kikkawa, T. Watamura, T. Niizeki, R. Ramos, E. Saitoh, and H. Murakami, Appl. Phys. Lett. **113**, 262402 (2018).

¹⁶⁴M. Agrawal, V. I. Vasyuchka, A. A. Serga, A. Kirihara, P. Pirro, T. Langner, M. B. Jungfleisch, A. V. Chumak, E. T. Papaioannou, and B. Hillebrands, Phys. Rev. B **89**, 224414 (2014).

¹⁶⁵N. Roschewsky, M. Schreier, A. Kamra, F. Schade, K. Ganzhorn, S. Meyer, H. Huebl, S. Geprägs, R. Gross, and S. T. B. Goennenwein, Appl. Phys. Lett. **104**, 202410 (2014).

¹⁶⁶T. Hioki, R. Iguchi, Z. Qiu, D. Hou, K. Uchida, and E. Saitoh, Appl. Phys. Express **10**, 073002 (2017).

¹⁶⁷J. M. Bartell, C. L. Jermain, S. V. Aradhya, J. T. Brangham, F. Yang, D. C. Ralph, and G. D. Fuchs, Phys. Rev. Appl. **7**, 044004 (2017).

¹⁶⁸J. Kimling, G.-M. Choi, J. T. Brangham, T. Matalla-Wagner, T. Huebner, T. Kuschel, F. Yang, and D. G. Cahill, Phys. Rev. Lett. **118**, 057201 (2017).

¹⁶⁹T. S. Seifert, S. Jaiswal, J. Barker, S. T. Weber, I. Razdolski, J. Cramer, O. Gueckstock, S. F. Maehrlein, L. Nadvornik, S. Watanabe, C. Ciccarelli, A. Melnikov, G. Jakob, M. Münzenberg, S. T. B. Goennenwein, G. Woltersdorf, B. Rethfeld, P. W. Brouwer, M. Wolf, M. Kläui, and T. Kampfrath, Nat. Commun. **9**, 2899 (2018).

¹⁷⁰T. Kikkawa, K. Uchida, Y. Shiomi, Z. Qiu, D. Hou, D. Tian, H. Nakayama, X.-F. Jin, and E. Saitoh, Phys. Rev. Lett. **110**, 067207 (2013).

¹⁷¹D. Qu, S. Y. Huang, J. Hu, R. Wu, and C. L. Chien, Phys. Rev. Lett. **110**, 067206 (2013).

¹⁷²T. Kikkawa, K. Uchida, S. Daimon, Y. Shiomi, H. Adachi, Z. Qiu, D. Hou, X.-F. Jin, S. Maekawa, and E. Saitoh, Phys. Rev. B **88**, 214403 (2013).

¹⁷³M. Schreier, G. E. W. Bauer, V. I. Vasyuchka, J. Flipse, K. Uchida, J. Lotze, V. Lauer, A. V. Chumak, A. A. Serga, S. Daimon, T. Kikkawa, E. Saitoh, B. J. van Wees, B. Hillebrands, R. Gross, and S. B. Goennenwein, J. Phys. D: Appl. Phys. **48**, 025001 (2015).

¹⁷⁴N. Vlietstra, J. Shan, B. J. van Wees, M. Isasa, F. Casanova, and J. B. Youssef, Phys. Rev. B **90**, 174436 (2014).

¹⁷⁵B. F. Miao, S. Y. Huang, D. Qu, and C. L. Chien, AIP Adv. **6**, 015018 (2016).

¹⁷⁶T. Kikkawa, M. Suzuki, J. Okabayashi, K. Uchida, D. Kikuchi, Z. Qiu, and E. Saitoh, Phys. Rev. B **95**, 214416 (2017).

¹⁷⁷F.-J. Chang, J. G. Lin, and S.-Y. Huang, Phys. Rev. Mater. **1**, 031401(R) (2017).

¹⁷⁸C. O. Avci, K. Garello, J. Mendil, A. Ghosh, N. Blasakis, M. Gabureac, M. Trassin, M. Fiebig, and P. Gambardella, Appl. Phys. Lett. **107**, 192405 (2015).

¹⁷⁹A. Sola, P. Bougiatioti, M. Kuepferling, D. Meier, G. Reiss, M. Pasquale, T. Kuschel, and V. Basso, Sci. Rep. **7**, 46752 (2017).

¹⁸⁰A. Sola, V. Basso, M. Kuepferling, M. Pasquale, D. Meier, G. Reiss, T. Kuschel, T. Kikkawa, K. Uchida, E. Saitoh, H. Jin, S. J. Watzman, S. Boona, J. Heremans, and M. B. Jungfleisch, IEEE Trans. Instrum. Meas. **68**, 1765 (2019).

¹⁸¹G. Venkat, C. D. W. Cox, A. Sola, V. Basso, and K. Morrison, Rev. Sci. Instrum. **91**, 073910 (2020).

¹⁸²H. Man, Z. Shi, G. Xu, Y. Xu, X. Chen, S. Sullivan, J. Zhou, K. Xia, J. Shi, and P. Dai, Phys. Rev. B **96**, 100406(R) (2017).

¹⁸³A. J. Princep, R. A. Ewings, S. Ward, S. Tóth, C. Dub, D. Prabhakaran, and A. T. Boothroyd, npj Quantum Mater. **2**, 63 (2017).

¹⁸⁴S. Shamoto, T. U. Ito, H. Onishi, H. Yamauchi, Y. Inamura, M. Matsuura, M. Akatsu, K. Kodama, A. Nakao, T. Moyoshi, K. Munakata, T. Ohhara, M. Nakamura, S. Ohira-Kawamura, Y. Némoto, and K. Shibata, Phys. Rev. B **97**, 054429 (2018).

¹⁸⁵Y. Nambu, J. Barker, Y. Okino, T. Kikkawa, Y. Shiomi, M. Enderle, T. Weber, B. Winn, M. Graves-Brook, J. Tranquada, T. Ziman, M. Fujita, G. E. W. Bauer, E. Saitoh, and K. Kakurai, Phys. Rev. Lett. **125**, 027201 (2020).

¹⁸⁶M. Agrawal, V. I. Vasyuchka, A. A. Serga, A. D. Karenowska, G. A. Melkov, and B. Hillebrands, Phys. Rev. Lett. **111**, 107204 (2013).

¹⁸⁷K. An, K. S. Olsson, A. Weathers, S. Sullivan, X. Chen, X. Li, L. G. Marshall, X. Ma, N. Klimovich, J. Zhou, L. Shi, and X. Li, Phys. Rev. Lett. **117**, 107202 (2016).

¹⁸⁸L. J. Cornelissen, K. J. H. Peters, G. E. W. Bauer, R. A. Duine, and B. J. van Wees, Phys. Rev. B **94**, 014412 (2016).

¹⁸⁹K. S. Olsson, K. An, G. A. Fiete, J. Zhou, L. Shi, and X. Li, Phys. Rev. X **10**, 021029 (2020).

¹⁹⁰S. Seki, T. Ideue, M. Kubota, Y. Kozuka, R. Takagi, M. Nakamura, Y. Kaneko, M. Kawasaki, and Y. Tokura, Phys. Rev. Lett. **115**, 266601 (2015).

¹⁹¹W. Yuan, Q. Zhu, T. Su, Y. Yao, W. Xing, Y. Chen, Y. Ma, X. Lin, J. Shi, R. Shindou, X. C. Xie, and W. Han, Sci. Adv. **4**, eaat1098 (2018).

¹⁹²J. Li, H. T. Simensen, D. Reitz, Q. Sun, W. Yuan, C. Li, Y. Tserkovnyak, A. Brataas, and J. Shi, Phys. Rev. Lett. **125**, 217201 (2020).

¹⁹³W. Yuan, J. Li, and J. Shi, Appl. Phys. Lett. **117**, 100501 (2020).

¹⁹⁴Y. Luo, C. Liu, H. Saglam, Y. Li, W. Zhang, S. S.-L. Zhang, J. E. Pearson, B. Fisher, T. Zhou, A. Bhattacharya, and A. Hoffmann, Phys. Rev. B **103**, L020401 (2021).

¹⁹⁵P. Muduli, R. Schlitz, T. Kosub, R. Hübner, A. Erbe, D. Makarov, and S. T. B. Goennenwein, APL Mater. **9**, 021122 (2021).

¹⁹⁶S. M. Wu, W. Zhang, A. Kc, P. Borisov, J. E. Pearson, J. S. Jiang, D. Lederman, A. Hoffmann, and A. Bhattacharya, Phys. Rev. Lett. **116**, 097204 (2016).

¹⁹⁷J. Li, Z. Shi, V. H. Ortiz, M. Aldosary, C. Chen, V. Aji, P. Wei, and J. Shi, Phys. Rev. Lett. **122**, 217204 (2019).

¹⁹⁸R. Lebrun, A. Ross, S. A. Bender, A. Qaiumzadeh, L. Baldrati, J. Cramer, A. Brataas, R. A. Duine, and M. Kläui, Nature **561**, 222 (2018).

¹⁹⁹A. Ross, R. Lebrun, M. Evers, A. Deák, L. Szunyogh, U. Nowak, and Kläui, Phys. Rev. B **103**, 224433 (2021).

²⁰⁰J. Holanda, D. S. Maior, O. Alves Santos, L. H. Vilela-Leão, J. B. S. Mendes, A. Azevedo, R. L. Rodriguez-Suárez, and S. M. Rezende, Applied Physics Letters **111**, 172405 (2017).

²⁰¹P. R. T. Ribeiro, F. L. A. Machado, M. Gamino, A. Azevedo, and S. M. Rezende, Phys. Rev. B **99**, 094432 (2019).

²⁰²I. Gray, T. Moriyama, N. Sivadas, G. M. Stiehl, J. T. Heron, R. Need, B. J. Kirby, D. H. Low, K. C. Nowack, D. G. Schlom, D. C. Ralph, T. Ono, and G. D. Fuchs, Phys. Rev. X **9**, 041016 (2019).

²⁰³G. R. Hoogeboom and B. J. van Wees, Phys. Rev. B **102**, 214415 (2020).

²⁰⁴Y. Shiomi, R. Takashima, D. Okuyama, G. Gitgeatpong, P. Piyawongwathanaka, K. Matan, T. J. Sato, and E. Saitoh, Phys. Rev. B **96**, 180414(R) (2017).

²⁰⁵W. Xing, L. Qiu, X. Wang, Y. Yao, Y. Ma, R. Cai, S. Jia, X. C. Xie, and W. Han, Phys. Rev. X **9**, 011026 (2019).

²⁰⁶G. Chen, S. Qi, J. Liu, D. Chen, J. Wang, S. Yan, Y. Zhang, S. Cao, M. Lu, S. Tian, K. Chen, P. Yu, Z. Liu, X. C. Xie, J. Xiao, R. Shindou, and J.-H. Chen, Nat. Commun. **12**, 6279 (2021).

²⁰⁷D. Hong, C. Liu, J. E. Pearson, A. Hoffmann, D. D. Fong, and A. Bhattacharya, Appl. Phys. Lett. **114**, 242403 (2019).

²⁰⁸A. Das, V. E. Phanindra, A. J. Watson, and T. Banerjee, Appl. Phys. Lett. **118**, 052407 (2021).

²⁰⁹S. Das, A. Ross, X. X. Ma, S. Becker, C. Schmitt, F. van Duijn, E. F. Galindez-Ruales, F. Fuhrmann, M. A. Syskaki, U. Ebels, V. Baltz, A. L. Barra, H. Y. Chen, G. Jakob, S. X. Cao, J. Sinova, O. Gomonay, R. Lebrun, and M. Kläui, Nat. Commun. **13**, 6140 (2022).

²¹⁰W. Lin, J. He, B. Ma, M. Matzelle, J. Xu, J. Freeland, Y. Choi, D. Haskel, B. Barbiellini, A. Bansil, G. A. Fiete, J. Zhou, and C. L. Chien, Nat. Phys. **18**, 800 (2022).

²¹¹J. Xu, J. He, J.-S. Zhou, D. Qu, S.-Y. Huang, and C. L. Chien, Phys. Rev. Lett. **129**, 117202 (2022).

²¹²G. R. Hoogeboom, T. Kuschel, G. E. W. Bauer, M. V. Mostovoy, A. V. Kimel, and B. J. van Wees, Phys. Rev. B **103**, 134406 (2021).

²¹³E. Parsonnet, L. Caretta, V. Nagarajan, H. Zhang, H. Taghinejad, P. Behera, X. Huang, P. Kavle, A. Fernandez, D. Nikonorov, H. Li, I. Young, J. Analytis, and R. Ramesh, Phys. Rev. Lett. **129**, 087601 (2022).

²¹⁴S. M. Rezende, R. L. Rodríguez Suárez, and A. Azevedo, Phys. Rev. B **93**, 014425 (2016).

²¹⁵Y. Yamamoto, M. Ichioka, and H. Adachi, Phys. Rev. B **100**, 064419 (2019).

²¹⁶D. Reitz, J. Li, W. Yuan, J. Shi, and Y. Tserkovnyak, Phys. Rev. B **102**, 020408(R) (2020).

²¹⁷Y. Yamamoto, M. Ichioka, and H. Adachi, Phys. Rev. B **105**, 104417 (2022).

²¹⁸N. Ito, T. Kikkawa, J. Barker, D. Hirobe, Y. Shiomi, and E. Saitoh, Phys. Rev. B **100**, 060402(R) (2019).

²¹⁹T. J. Williams, A. A. Aczel, M. D. Lumsden, and S. E. Nagler, Phys. Rev. B **92**, 144404 (2015).

²²⁰T. Liu, J. Peiro, D. K. de Wal, J. C. Leutenantsmeyer, M. H. D. Guimarães, and B. J. van Wees, Phys. Rev. B **101**, 205407 (2020).

²²¹S.-K. Lee, W.-Y. Lee, T. Kikkawa, C. T. Le, M.-S. Kang, G.-S. Kim, A. D. Nguyen, Y. S. Kim, N.-W. Park, and E. Saitoh, Adv. Func. Mater. **30**, 2003192 (2020).

²²²L. J. Cornelissen, K. Oyanagi, T. Kikkawa, Z. Qiu, T. Kuschel, G. E. W. Bauer, B. J. van Wees, and E. Saitoh, Phys. Rev. B **96**, 104441 (2017).

²²³K. Oyanagi, T. Kikkawa, and E. Saitoh, AIP Adv. **10**, 015031 (2020).

²²⁴Z. Shi, Q. Xi, J. Li, Y. Li, M. Aldosary, Y. Xu, J. Zhou, S.-M. Zhou, and J. Shi, Phys. Rev. Lett. **127**, 277203 (2021).

²²⁵T. Kikkawa, K. Oyanagi, T. Hioki, M. Ishida, Z. Qiu, R. Ramos, Y. Hashimoto, and E. Saitoh, Phys. Rev. Mater. **6**, 104402 (2022).

²²⁶W. Xing, Y. Ma, Y. Yao, R. Cai, Y. Ji, R. Xiong, K. Shen, and W. Han, Phys. Rev. B **102**, 184416 (2020).

²²⁷J. Shan, A. V. Singh, L. Liang, L. J. Cornelissen, Z. Galazka, A. Gupta, B. J. van Wees, and T. Kuschel, Appl. Phys. Lett. **113**, 162403 (2018).

²²⁸H. Wang, D. Hou, T. Kikkawa, R. Ramos, K. Shen, Z. Qiu, Y. Chen, M. Umeda, Y. Shiomi, X. Jin, and E. Saitoh, Appl. Phys. Lett. **112**, 142406 (2018).

²²⁹R. Ramos, T. Hioki, Y. Hashimoto, T. Kikkawa, P. Frey, A. J. E. Kreil, V. I. Vasyuchka, A. A. Serga, B. Hillebrands, and E. Saitoh, Nat. Commun. **10**, 5162 (2019).

²³⁰B. Yang, S. Y. Xia, H. Zhao, G. Liu, J. Du, K. Shen, Z. Qiu, and D. Wu, Phys. Rev. B **103**, 054411 (2021).

²³¹B. Z. Rameshti and R. A. Duine, Phys. Rev. B **99**, 060402(R) (2019).

²³²R. Schmidt, F. Wilken, T. S. Nunner, and P. W. Brouwer, Phys. Rev. B **98**, 134421 (2018).

²³³D. Hirobe, M. Sato, T. Kawamata, Y. Shiomi, K. Uchida, R. Iguchi, Y. Koike, S. Maekawa, and E. Saitoh, Nat. Phys. **13**, 30 (2017).

²³⁴D. Hirobe, T. Kawamata, K. Oyanagi, Y. Koike, and E. Saitoh, J. Appl. Phys. **123**, 123903 (2018).

²³⁵Y. Chen, M. Sato, Y. Tang, Y. Shiomi, K. Oyanagi, T. Masuda, Y. Nambu, M. Fujita, and E. Saitoh, Nat. Commun. **12**, 5199 (2021).

²³⁶W. Xing, R. Cai, K. Moriyama, K. Nara, Y. Yao, W. Qiao, K. Yoshimura, and W. Han, Appl. Phys. Lett. **120**, 042402 (2022).

²³⁷S. M. Rezende, J. Appl. Phys. **132**, 091101 (2022).

²³⁸T. Kikkawa, D. Reitz, H. Ito, T. Makiuchi, T. Sugimoto, K. Tsunekawa, S. Daimon, K. Oyanagi, R. Ramos, S. Takahashi, Y. Shiomi, Y. Tserkovnyak, and E. Saitoh, Nat. Commun. **12**, 4356 (2021).

²³⁹Y. Shiomi, J. Lustikova, S. Watanabe, D. Hirobe, S. Takahashi, and E. Saitoh, Nat. Phys. **15**, 22 (2019).

²⁴⁰J. Korringa, Physica **16**, 601 (1950).

²⁴¹J. Flipse, F. K. Dejene, D. Wagenaar, G. E. W. Bauer, J. B. Youssef, and B. J. van Wees, Phys. Rev. Lett. **113**, 027601 (2014).

²⁴²R. Itoh, R. Iguchi, S. Daimon, K. Oyanagi, K. Uchida, and E. Saitoh, Phys. Rev. B **96**, 184422 (2017).

²⁴³S. Daimon, R. Iguchi, T. Hioki, E. Saitoh, and K. Uchida, Nat. Commun. **7**, 13754 (2016).

²⁴⁴S. Daimon, K. Uchida, R. Iguchi, T. Hioki, and E. Saitoh, Phys. Rev. B **96**, 024424 (2017).

²⁴⁵K. Uchida, R. Iguchi, S. Daimon, R. Ramos, A. Anadón, I. Lucas, P. A. Algarabel, L. Morellón, M. H. Aguirre, M. R. Ibarra, and E. Saitoh, Phys. Rev. B **95**, 184437 (2017).

²⁴⁶T. Seki, R. Iguchi, K. Uchida, and K. Takanashi, Appl. Phys. Lett. **112**, 152403 (2018).

²⁴⁷A. Yagmur, R. Iguchi, S. Geprägs, A. Erb, S. Daimon, E. Saitoh, R. Gross, and K. Uchida, J. Phys. D: Appl. Phys. **51**, 194002 (2018).

²⁴⁸S. Daimon, K. Uchida, N. Ujjie, Y. Hattori, R. Tsuboi, and E. Saitoh, Appl. Phys. Express **13**, 103001 (2020).

²⁴⁹T. Yamazaki, R. Iguchi, T. Ohkubo, H. Nagano, and K. Uchida, Phys. Rev. B **101**, 020415(R) (2020).

²⁵⁰A. Sola, V. Basso, M. Kuepferling, C. Dubs, and M. Pasquale, Sci. Rep. **9**, 2047 (2019).

²⁵¹Y. Ohnuma, M. Matsuo, and S. Maekawa, Phys. Rev. B **96**, 134412 (2017).

²⁵²V. Basso, M. Kuepferling, A. Sola, P. Ansalone, and M. Pasquale, IEEE Magn. Lett. **9**, 3104704 (2018).

²⁵³S. J. Barnett, Rev. Mod. Phys. **7**, 129 (1935).

²⁵⁴G. G. Scott, Rev. Mod. Phys. **34**, 102 (1962).

²⁵⁵R. Huguenin and D. Baldock, Phys. Rev. Lett. **16**, 795 (1966).

²⁵⁶R. Huguenin, G. P. Pells, and D. N. Baldock, J. Physics F: Metal Physics **1**, 281 (1971).

²⁵⁷L. D. Landau and E. M. Lifshitz, *Mechanics*, 3rd ed., Course of Theoretical Physics, Vol. 1 (Butterworth-Heinemann, Oxford, 1976).

²⁵⁸F. W. Hehl, P. von der Heyde, G. D. Kerlick, and J. M. Nester, Rev. Mod. Phys. **48**, 393 (1976).

²⁵⁹F. W. Hehl and W.-T. Ni, Phys. Rev. D **42**, 2045 (1990).

²⁶⁰K. Harii, Y.-J. Seo, Y. Tsutsumi, H. Chudo, K. Oyanagi, M. Matsuo, Y. Shiomi, T. Ono, S. Maekawa, and E. Saitoh, Nat. Commun. **10**, 2616 (2019).

²⁶¹G. Zolfagharkhani, A. Gaidarzy, P. Degiovanni, S. Kettemann, P. Fulde, and P. Mohanty, Nat. Nanotechnol. **3**, 720 (2008).

²⁶²R. Takahashi, M. Matsuo, M. Ono, K. Harii, H. Chudo, S. Okayasu, J. Ieda, S. Takahashi, S. Maekawa, and E. Saitoh, Nat. Phys. **12**, 52 (2015).

²⁶³R. Takahashi, H. Chudo, M. Matsuo, K. Harii, Y. Ohnuma, S. Maekawa, and E. Saitoh, Nat. Commun. **11**, 3009 (2020).

²⁶⁴D. Kobayashi, T. Yoshikawa, M. Matsuo, R. Iguchi, S. Maekawa, E. Saitoh, and Y. Nozaki, Phys. Rev. Lett. **119**, 077202 (2017).

²⁶⁵H. Chudo, M. Ono, K. Harii, M. Matsuo, J. Ieda, R. Haruki, S. Okayasu, S. Maekawa, H. Yasuoka, and E. Saitoh, Appl. Phys. Express **7**, 063004 (2014).

²⁶⁶H. Chudo, K. Harii, M. Matsuo, J. Ieda, M. Ono, S. Maekawa, and E. Saitoh, J. Phys. Soc. Jpn. **84**, 043601 (2015).

²⁶⁷K. Harii, H. Chudo, M. Ono, M. Matsuo, J. Ieda, S. Okayasu, S. Maekawa, and E. Saitoh, Jpn. J. Appl. Phys. **54**, 050302 (2015).

²⁶⁸H. Chudo, M. Matsuo, S. Maekawa, and E. Saitoh, Phys. Rev. B **103**, 174308 (2021).

²⁶⁹A. Abragam, *The Principles of Nuclear Magnetism* (Oxford University Press, London, 1961).

²⁷⁰C. P. Slichter, *Principles of Magnetic Resonance*, edited by 3rd Enlarged and Updated (Springer, New York, 1996).

²⁷¹M. Arabgol and T. Sleator, Phys. Rev. Lett. **122**, 177202 (2019).

²⁷²J. Jeener, Appl. Phys. Express **13**, 109101 (2020).

²⁷³J. Frohlich and U. M. Studer, Rev. Mod. Phys. **65**, 733 (1993).

²⁷⁴H. Chudo, M. Matsuo, K. Harii, S. Maekawa, and E. Saitoh, Appl. Phys. Express **13**, 109102 (2020).

²⁷⁵L. D. Landau and E. M. Lifshitz, *Electrodynamics of Continuous Media*, 2nd ed., Course of Theoretical Physics, Vol. 8 (Butterworth-Heinemann, Oxford, 1984).

²⁷⁶E. L. Hahn, Lect. Notes Phys. **684**, 1 (2006).

²⁷⁷M. Ono, H. Chudo, K. Harii, S. Okayasu, M. Matsuo, J. Ieda, R. Takahashi, S. Maekawa, and E. Saitoh, Phys. Rev. B **92**, 174424 (2015).

²⁷⁸Y. Ogata, H. Chudo, M. Ono, K. Harii, M. Matsuo, S. Maekawa, and E. Saitoh, Appl. Phys. Lett. **110**, 072409 (2017).

²⁷⁹Y. Ogata, H. Chudo, B. Gu, N. Kobayashi, M. Ono, K. Harii, M. Matsuo, E. Saitoh, and S. Maekawa, J. Magn. Magn. Mater. **442**, 329 (2017).

²⁸⁰H. Masumoto, S. Takahashi, S. Maekawa, and N. Kobayashi, Nat. Commun. **5**, 4417 (2014).

²⁸¹R. A. Reck and D. L. Fry, Phys. Rev. **184**, 492 (1969).

²⁸²Y. Wu, J. Stöhr, B. D. Hermsmeier, M. G. Samant, and D. Weller, Phys. Rev. Lett. **69**, 2307 (1992).

²⁸³M. Imai, Y. Ogata, H. Chudo, M. Ono, K. Harii, M. Matsuo, Y. Ohnuma, S. Maekawa, and E. Saitoh, *Appl. Phys. Lett.* **113**, 052402 (2018).

²⁸⁴M. Imai, H. Chudo, M. Ono, K. Harii, M. Matsuo, Y. Ohnuma, S. Maekawa, and E. Saitoh, *Appl. Phys. Lett.* **114**, 162402 (2019).

²⁸⁵R. Pauthenet, *J. Appl. Phys.* **29**, 253 (1958).

²⁸⁶H. Chudo, M. Imai, M. Matsuo, S. Maekawa, and E. Saitoh, *J. Phys. Soc. Jpn.* **90**, 081003 (2021).

²⁸⁷M. Imai, H. Chudo, M. Matsuo, S. Maekawa, and E. Saitoh, *Phys. Rev. B* **102**, 014407 (2020).